Galaxy Zoo: Major Galaxy Mergers Are Not a Significant Quenching Pathway

William C. Keel – University of Alabama
et al.

Citation of published version:

Weigel, A., et al. (2017): Galaxy Zoo: Major Galaxy Mergers Are Not a Significant Quenching Pathway. *The Astrophysical Journal*, 845(2).
DOI: https://doi.org/10.3847/1538-4357/aa8097

The Astrophysical Journal, 845:145 (28pp), 2017 August 20 https://doi.org/10.3847/1538-4357/aa8097

Galaxy Zoo: Major Galaxy Mergers Are Not a Significant Quenching Pathway*

Anna K. Weigel[1], Kevin Schawinski[1], Neven Caplar[1], Alfredo Carpineti[2], Ross E. Hart[3], Sugata Kaviraj[4,5], William C. Keel[6], Sandor J. Kruk[7], Chris J. Lintott[7], Robert C. Nichol[8,10], Brooke D. Simmons[9], and Rebecca J. Smethurst[3,7]

[1] Institute for Astronomy, Department of Physics, ETH Zurich, Wolfgang-Pauli-Strasse 27, CH-8093 Zurich, Switzerland
[2] Blackett Laboratory, Imperial College London, London SW7 2AZ, UK
[3] School of Physics and Astronomy, The University of Nottingham, University Park, Nottingham NG7 2RD, UK
[4] Centre for Astrophysics Research, University of Hertfordshire, College Lane, Hatfield AL10 9 AB, UK
[5] Worcester College, Oxford, UK
[6] Department of Physics and Astronomy, University of Alabama, Box 879324, Tuscaloosa, AL 35487, USA
[7] Oxford Astrophysics, Denys Wilkinson Building, Keble Road, Oxford OX1 3RH, UK
[8] Institute of Cosmology & Gravitation, University of Portsmouth, Dennis Sciama Building, Portsmouth PO1 3FX, UK
[9] Center for Astrophysics and Space Sciences (CASS), Department of Physics, University of California, San Diego, CA 92093, USA
Received 2017 June 9; revised 2017 July 10; accepted 2017 July 16; published 2017 August 21

Abstract

We use stellar mass functions to study the properties and the significance of quenching through major galaxy mergers. In addition to SDSS DR7 and Galaxy Zoo 1 data, we use samples of visually selected major galaxy mergers and post-merger galaxies. We determine the stellar mass functions of the stages that we would expect major-merger-quenched galaxies to pass through on their way from the blue cloud to the red sequence: (1) major merger, (2) post-merger, (3) blue early type, (4) green early type, and (5) red early type. Based on their similar mass function shapes, we conclude that major mergers are likely to form an evolutionary sequence from star formation to quiescence via quenching. Relative to all blue galaxies, the major-merger fraction increases as a function of stellar mass. Major-merger quenching is inconsistent with the mass and environment quenching model. At $z \sim 0$, major-merger-quenched galaxies are unlikely to constitute the majority of galaxies that transition through the green valley. Furthermore, between $z \sim 0 - 0.5$, major-merger-quenched galaxies account for 1%–5% of all quenched galaxies at a given stellar mass. Major galaxy mergers are therefore not a significant quenching pathway, neither at $z \sim 0$ nor within the last 5 Gyr. The majority of red galaxies must have been quenched through an alternative quenching mechanism that causes a slow blue to red evolution.

Key words: galaxies: evolution – galaxies: interactions – galaxies: luminosity function, mass function

1. Introduction

The physical cause of the cessation of star formation is an open question in astrophysics today. In the local universe, galaxies fall into two broad categories: spiral or late-type galaxies, which mostly have a blue optical color, and elliptical or early-type galaxies, which are primarily optically red (but also see: Schawinski et al. 2009; Masters et al. 2010). In the color–mass and color–magnitude diagrams, galaxies separate into the "blue cloud" and the "red sequence" (Bell et al. 2003; Baldry et al. 2004; Martin et al. 2007; Taylor et al. 2015). Between the blue cloud and the red sequence lies the so-called "green valley" (Bell et al. 2003; Faber et al. 2007; Martin et al. 2007; Fang et al. 2012; Schawinski et al. 2014), a transition zone that contains both late- and early-type galaxies. Blue cloud galaxies are also often referred to as galaxies on the "main sequence" (Brinchmann et al. 2004; Daddi et al. 2007; Elbaz et al. 2007; Noeske et al. 2007; Salim et al. 2007; Peng et al. 2010; Lilly et al. 2013; Speagle et al. 2014; Lee et al. 2015; Kurczynski et al. 2016; Tomczak et al. 2016). In star formation rate (SFR) versus stellar mass space, they lie on an almost linear relation. Red early-type galaxies are quiescent. They have significantly lower SFRs than blue late types and thus lie below the main sequence. The bimodality in color–mass and color–magnitude space and the existence of the main sequence imply that blue galaxies are likely to shut down their star formation at some point during their lifetime. A significant decrease in the SFR causes them to transition from the blue cloud to the green valley and finally to the red sequence. In combination with a morphological transformation from spiral to elliptical, this evolution could explain the existence of the red sequence. We refer to the physical process that causes blue galaxies to shut down their star formation as quenching.

A variety of physical processes that could cause star formation quenching have been proposed. These can be classified into internal and external processes. Internal processes include AGN feedback (Silk & Rees 1998; Di Matteo et al. 2005; Schawinski et al. 2006; Kauffmann et al. 2007; Georgakakis et al. 2008; Cattaneo et al. 2009; Hickox et al. 2009; Fabian 2012; Bongiorno et al. 2016; Kaviraj et al. 2017) and secular processes (Kormendy & Kennicutt 2004; Masters et al. 2011; Cheung et al. 2013). Externally, quenching could be correlated with the environment (Gunn & Gott 1972; Larson et al. 1980; Balogh et al. 2000; Knobel et al. 2015; Peng et al. 2015; Woo et al. 2015) or with the occurrence of major galaxy mergers (Sanders et al. 1988; Mihos & Hernquist 1996; Di Matteo et al. 2005; Springel et al. 2005b; Croton et al. 2006; Hopkins et al. 2006, 2008b; Khalatyan et al. 2008; Somerville et al. 2008; Faisst et al. 2017). Of course, we could also imagine a combination of different processes. For example, Peng et al. (2010, hereafter P10) and Peng et al. (2012) use external ("environment quenching") and mass-dependent,

* This publication has been made possible by the participation of more than 100,000 volunteers in the Galaxy Zoo project. Their contributions are individually acknowledged at http://authors.galaxyzoo.org.
[10] South East Physics Network, http://www.sepnet.ac.uk.

likely internal ("mass quenching") processes to reproduce the stellar mass function of red galaxies with their phenomenological model.

Our aim is to study the classical quenching model based on major mergers. Mergers between gas-rich galaxies of comparable mass cause most of the galaxies' gas to be driven to the new center. This can ignite both a starburst and an AGN. Star formation and AGN feedback can expel the gas from the galaxy, preventing further star formation. The now elliptical galaxy leaves the blue cloud and crosses the green valley before settling on the red sequence (Sanders et al. 1988; Mihos & Hernquist 1996; Di Matteo et al. 2005; Springel et al. 2005b; Croton et al. 2006; Hopkins et al. 2006, 2008b; Khalatyan et al. 2008; Somerville et al. 2008).

We use stellar mass functions of galaxies that are transitioning from the blue cloud to the red sequence to study the properties and the significance of this quenching process. Stellar mass functions are an important statistical measure that allows us to study and infer the properties of a large sample of galaxies. Specifically, they allow us to probe if quenching through major mergers includes a mass dependence. Furthermore, we can constrain the relative amount of time spent in stages along the sequence and measure the merger fraction. By comparing the stellar mass function shapes of major mergers and red galaxies, we can also test if merger quenching can account for all quenched galaxies or if an additional quenching channel is necessary.

To construct these stellar mass functions, we rely on morphological classifications from Galaxy Zoo.[11] Besides the classifications from Galaxy Zoo 1 (GZ1; Lintott et al. 2008, 2011), we also use the major-merger sample by D10 (hereafter D10) and Darg et al. (2010b), and the post-merger sample by Carpineti et al. (2012). Our analysis is thus based on the visual classifications of over 100,000 Galaxy Zoo volunteers.

We determine the stellar mass functions of galaxies along the major-merger quenching sequence by using the method introduced in Weigel et al. (2016). This approach is based on the combination of three independent methods ($1/V_{\rm max}$: Schmidt 1968; STY: Sandage et al. 1979; SWML: Efstathiou et al. 1988). Blue, star-forming and red, quiescent galaxies are usually well fit by single and double Schechter functions, respectively (e.g., Li & White 2009; P10; Pozzetti et al. 2010; Baldry et al. 2012; Ilbert et al. 2013; Muzzin et al. 2013). Yet it is important to note that when fitting the stellar mass functions, we are not making any a priori assumptions on which galaxy subsample should be fit with a single and a double Schechter function. We use a likelihood ratio test to determine the better fitting model.

This paper is organized as follows. In Section 2, we introduce the galaxy, the major merger, and the post-merger sample, and give a brief overview of the stellar mass function method used in Weigel et al. (2016). Section 4 represents the first part of the paper and is purely data driven: we introduce the stellar mass functions of major mergers and post-mergers, determine the merger fraction, and test if our measurements are consistent with the phenomenological model by P10. In the second part of the paper, we use these stellar mass functions to investigate the process of major-merger quenching. First, we introduce and motivate our assumptions in Section 4. Second, in Section 5, we apply these assumptions to our measurements. This is followed by a discussion and a summary in Sections 6 and 7, respectively.

Throughout this paper, we assume a ΛCDM cosmology with $h_0 = 0.7$, $\Omega_{\rm m} = 0.3$ and $\Omega_\Lambda = 0.7$ (Komatsu et al. 2011).

2. Data

2.1. The SDSS Galaxy Sample

For our analysis, we use data from the seventh data release (DR7) of the Sloan Digital Sky Survey (SDSS; York et al. 2000; Abazajian et al. 2009). We extract spectroscopic redshift and magnitude values from the New York Value-Added Galaxy Catalog (NYU VAGC; Blanton et al. 2005; Padmanabhan et al. 2008). For the stellar mass measurements, we use those of Brinchmann et al. (2004) recorded in the Max Planck Institute for Astrophysics John Hopkins University (MPA JHU; Kauffmann et al. 2003; Brinchmann et al. 2004; Salim et al. 2007) catalog. These stellar mass estimates are based on fits to the photometry and model spectra by Bruzual & Charlot (2003) and are in good agreement to the 4000 Å- and $H\delta_A$-based measurements by Kauffmann et al. (2003).[12]

We cross-match to the GZ1 catalog[13] (Table 2 in Lintott et al. 2011; also see Lintott et al. 2008; Land et al. 2008) to obtain morphological classifications for all galaxies. Each object in the sample was classified 38 times on average by over 100,000 Galaxy Zoo volunteers. GZ1[14] users were given six possible classifications for each galaxy ("Elliptical galaxy," "Clockwise/Z-wise spiral galaxy," "Anti-clockwise/S-wise spiral galaxy," "Spiral galaxy other (e.g., edge on)," "Star or do not know," "Merger"). These can be summarized into "elliptical" (E) and "combined spiral" (CS = "Clockwise/Z-wise spiral galaxy" + "Anti-clockwise/S-wise spiral galaxy" + "Spiral galaxy other (e.g., edge on)") galaxies. The likelihood of a galaxy having a spiral or an elliptical morphology depends on the fraction of users that have classified the galaxy as such. This is referred to as the vote fraction.

We base our analysis on the "elliptical," "spiral," and "uncertain" type flags. These flags are based on vote distributions that have been corrected for classification bias (Bamford et al. 2009; see Willett et al. 2013 and Hart et al. 2016 for Galaxy Zoo 2). High-redshift galaxies are more likely to be categorized as ellipticals since they appear fainter and smaller, which make it more difficult for the classifier to recognize morphological features. To correct for this effect, elliptical and combined spiral galaxies with raw vote fractions above 80% are chosen to compute the elliptical-to-spiral ratio. The raw vote distributions are then debiased by assuming that there is no redshift evolution in this morphological ratio within bins of luminosity and size. Galaxies with debiased vote fractions above 80% in the elliptical and spiral categories are then flagged as "elliptical" and "spiral," respectively. Galaxies for which the debiased vote fractions in both the elliptical and the combined spiral category lie below 80% are flagged as "uncertain." We note that the GZ1 interface did not allow users to classify galaxies as "uncertain." The "uncertain" flag simply reflects the fact that a galaxy's spiral and elliptical probabilities lie below the corresponding thresholds. Schawinski et al. (2014) argue that the majority of galaxies in the "uncertain" category show late-type characteristics, whereas only a small fraction might be misclassified early types. By using a high debiased vote fraction cut of 80%, we eliminate some of

[11] http://www.galaxyzoo.org

[12] http://wwwmpa.mpa-garching.mpg.de/SDSS/DR7/mass_comp.html

[13] http://data.galaxyzoo.org

[14] http://zoo1.galaxyzoo.org/

the nuances in galaxy morphologies. However, the resulting clean early-type sample allows the inference of a broad picture of galaxy evolution. We refer to galaxies that are flagged as "elliptical," "spiral," and "uncertain" as early types, late types, and indeterminates.

To be able to correct for dust, we use the absorption- and emission-line measurements from OSSY (Oh et al. 2011). As an environment estimate, we include the overdensity measurements from Weigel et al. (2016), which are based on a fifth nearest neighbor approach ($M > 10^9\,M_\odot$, recession velocity range $\pm$1000km/s). We also add halo mass measurements, spectral completeness values, and the classification into centrals and satellites from the Yang et al. (2007) catalog. We limit our main sample to the redshift range between 0.02 and 0.06 and to objects of the MPA JHU spectral type "GALAXY." We refer to the sample of galaxies that lie within this redshift range, have the correct spectroscopic classification, and for which stellar masses, morphological classifications, and environment and emission-line measurements are available as the "entire galaxy sample." For more details on this sample and the overdensity measurement, see Weigel et al. (2016).

2.2. Color Cuts

We use the color–mass diagram (Bell et al. 2003; Baldry et al. 2004; Faber et al. 2007; Martin et al. 2007; Schawinski et al. 2014) to split our sample into red, green, and blue galaxies. We use the Petrosian flux values from the NYU VAGC and apply a dust and k-correction. We k-correct to redshift zero using the KCORRECT IDL package (version 4.2) by Blanton & Roweis (2007) and use the Calzetti law (Calzetti et al. 2000) with $E(B-V)$ values from OSSY ([EBV_STAR]; Oh et al. 2011) to correct for internal dust extinction. We show the color–mass diagram for our main sample in Figure 1.

We use the color definitions from Weigel et al. (2016) and refer to sources lying above,

$$u - r\ (\log M) = 0.6 + 0.15 \times \log M, \quad (1)$$

as being red and to galaxies below,

$$u - r\ (\log M) = 0.15 + 0.15 \times \log M, \quad (2)$$

as being blue. Objects between Equations (1) and (2) are part of the green valley (Bell et al. 2004; Martin et al. 2007; Fang et al. 2012; Schawinski et al. 2014) and are referred to as being green.

The color–mass diagram in Figure 1 illustrates that splitting the sample by color and morphology yields different results. Not all early types are red (Schawinski et al. 2009) and not all late types are blue (Masters et al. 2010).

2.3. The Major Merger Sample

We use the Galaxy Zoo merger sample by D10 and Darg et al. (2010b). The sample is based on SDSS DR6 and contains 3003 visually classified merging systems in the redshift range 0.005–0.1.

D10 based their sample on the GZ1 morphological classifications (see Section 2.1). For each source, D10 calculated the ratio of the number of people who classified this objects as a merger to the total number of classifications of this source. The weighted-merger vote fraction f_m of this object is then defined as this ratio multiplied by a weighting factor that represents the reliability of all users that classified the object. If f_m is equal to its minimum value 0, the galaxy is unlikely to be a merger. If f_m is equal to its maximum value 1, the galaxy has consistently been classified as a merger. In their catalog, D10 only include galaxies for which $f_\mathrm{m} > 0.4$.

D10 determine stellar masses for all galaxies in their sample by fitting two-component star formation histories to the photometry. These fits are based on Maraston (1998, 2005) stellar models, a Salpeter (Salpeter 1955) initial mass function, stellar populations with fixed solar metallicity and variable ages, and a dust implementation according to the Calzetti law (Calzetti et al. 2000). SDSS spectra and thus MPA JHU (Kauffmann et al. 2003; Brinchmann et al. 2004; Salim et al. 2007) stellar mass measurements for both galaxies involved in the merger are only available for 23% of all merging systems in the D10 catalog. We thus use the photometry-based stellar mass measurements by D10 to restrict ourselves to mergers between galaxies with a mass ratio within $1/3 < M_1/M_2 < 3$.

While we use the stellar mass estimates by D10 to select major mergers, we use the stellar mass values by Brinchmann et al. (2004) to construct the major-merger mass function to ensure consistency with the other mass functions presented here. If spectra are available for both merging galaxies, we consider the mass of the more massive merging partner in the construction of the major merger mass function. If only one of the two sources has been observed spectroscopically, we take the mass of the source with an available spectrum into account. According to the D10 mass measurements, this corresponds to the more massive merging partner in 69% of all merging systems with one spectrum. We discuss the effect of this approach on the merger mass function shape in Appendix A .1.

D10 find that their sample of merging galaxies contains three times as many spiral as elliptical galaxies and is dominated by mergers between spiral galaxies. In the general galaxy population, the ratio of spirals to ellipticals is 3:2 for the same redshift range and above the same magnitude limit. Willett et al. (2015) show that on average the D10 merging galaxies pairs lie $\sim$0.3 dex above the main sequence relation. Using the color definitions introduced in Section 2.2, we classify $\sim$55% of all major-merger galaxies in our sample as blue. We thus conclude that the majority of merging galaxies in the D10 sample are blue, star-forming spirals.

Galaxy pairs that seem to be merging due to projection effects can easily be eliminated if spectroscopic redshifts are available for both galaxies. When only one of the merging galaxies has an available spectrum, the major-merger candidate has to be visually examined for galaxy interactions. D10 argue that galaxies with $f_\mathrm{m} > 0.4$ are predominantly clear major mergers and that decisions regarding possible projection effects only have to be made in rare cases. Stellar projections are excluded based on the SDSS PHOTOTAG "type" classification which indicates whether the possible merging partner is point-like or extended.

2.4. The Post-merger Sample

In the construction of their major merger sample, D10 flag objects that were classified as being a major merger by the Galaxy Zoo users and only show a single core. These objects are identified as a single source by SDSS but show strong perturbations in the outskirts. They are therefore likely to be objects in the late stages of a merger. D10 flag these objects that can no longer be resolved by the SDSS pipeline as "post-mergers." Strong perturbations in the periphery can also

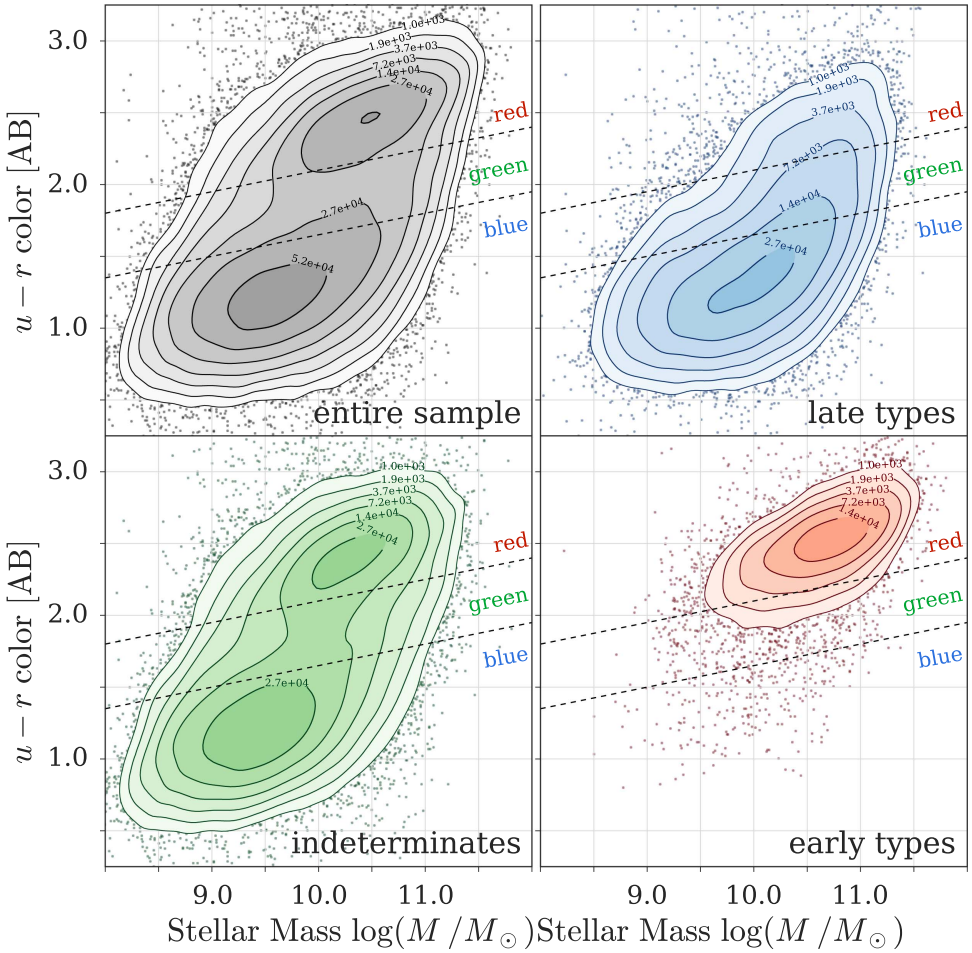

Figure 1. Color–mass diagrams for the entire galaxy sample, indeterminates, and late and early types. All colors are dust and *k*-corrected. The dashed lines indicate our definition of the green valley (Equations (1) and (2)). Out of the ∼110,000 objects in the entire galaxy sample, 33.29% and 8.44% are classified as being late- and early-type galaxies, respectively. For the remaining galaxies, the probability of being a late- or an early-type galaxy lies below the vote fraction threshold. They are categorized as indeterminate. This figure illustrates that splitting the sample by color is not equivalent to splitting the sample by morphology since not all late-type galaxies are blue (Masters et al. 2010) and not all early-type galaxies are red (Schawinski et al. 2009). The contours represent equal steps in log space and show the number of objects.

be caused by a close encounter with a second galaxy that is no longer in the field of view. These objects are flagged as "fly-bys." While D10 do not include these perturbed systems in their major-merger catalog, Carpineti et al. (2012) investigate the color and AGN activity of "post-merger" flagged sources relative to early-type galaxies. We refer to galaxies in the Carpineti et al. (2012) sample as post-mergers.

Carpineti et al. (2012) select a sample of spheroidal post-mergers and argue that ∼55% of sources in this sample are remnants of merging systems that involved at least one late-type galaxy. According to our color definitions, ∼87% are defined as blue.

We note that the major-merger and post-merger samples are based on SDSS DR6, while the rest of our analysis is based on SDSS DR7. The galaxies of the SDSS DR6 spectroscopic sample make up ∼85% of the galaxies in the SDSS DR7 spectroscopic sample.[15] Assuming there is no bias in the way the additional galaxies in DR7 were selected, we would expect to find ∼15% more major-merger and post-merger galaxies if we select them in the same way from DR7 instead of DR6. For the major-merger and post-merger mass functions, which we will determine below, this would result in a constant increase in the normalization by ∼0.06 dex. Using SDSS DR6 instead of SDSS DR7 data for the major-merger and post-merger sample therefore does not significantly affect our results.

2.5. Stellar Mass Function Construction

To construct stellar mass functions, we follow Weigel et al. (2016) and combine the classical $1/V_{\rm max}$ approach developed by Schmidt (1968) with the parametric maximum likelihood method by Sandage et al. (1979, STY) and the non-parametric step-wise maximum likelihood method (SWML), which was established by Efstathiou et al. (1988).

In STY, we are assuming that the stellar mass function can be modeled by either a single or a double Schechter function (Schechter 1976). We estimate the likelihood of both functional forms and use a likelihood ratio test to determine which model provides a better description of the data.

In the figures below, we show the $1/V_{\rm max}$ and SWML results with open and filled symbols, respectively. Upper limits according to the two methods are shown with arrows of the same style. The best-fitting Schechter functions according to the STY method are illustrated with solid lines. The corresponding 1σ errors are shown as shaded regions.

[15] See http://classic.sdss.org/dr6/ and http://classic.sdss.org/dr7/.

We define the single Schechter function as

$$\Phi\, d\log M = \ln(10)\Phi^* e^{-M/M^*}\left(\frac{M}{M^*}\right)^{\alpha+1} d\log M, \quad (3)$$

and use the following definition for the double Schechter function:

$$\Phi\, d\log M = \ln(10) e^{-M/M^*} \times \left[\Phi_1^*\left(\frac{M}{M^*}\right)^{\alpha_1+1} + \Phi_2^*\left(\frac{M}{M^*}\right)^{\alpha_2+1}\right] d\log M. \quad (4)$$

Note that the ln 10 factor and the +1 in the exponent of M/M^* is due to the conversion from dM to $d\log M$.

For each sample, we determine the stellar mass completeness as a function of redshift using the technique introduced by Pozzetti et al. (2010). This approach is based on keeping the mass-to-light ratio of each individual source constant and determining the stellar mass that this object would have if its redshift stayed constant, but its flux was equal to the magnitude limit.

For the $1/V_{\rm max}$ approach we determine the stellar mass completeness of each subsample and subsequently the $V_{\rm max}$ values of each source by using the approach by Pozzetti et al. (2010). To be able to apply the STY and the SWML method, we also estimate the minimum stellar mass at which each galaxy would still be part of the sample. We do so by keeping the mass-to-light ratio constant and scaling the flux down to the r-band flux limit.

Weigel et al. (2016) show that the three independent mass function estimators deviate at the low-mass end. Compared to STY and SWML, the $1/V_{\rm max}$ technique tends to overestimate Φ (also see Efstathiou et al. 1988 and Willmer 1997) and depends strongly on the shape of the stellar mass completeness function. While STY and SWML might be less commonly used mass function estimators, they have the advantage that the Φ values in different mass bins are not independent from each other. This makes these two techniques more robust toward deviations in the mass completeness function. For a more detailed discussion of each of the mass function estimators, their advantages, and the disadvantages and systematics that might affect them, see Weigel et al. (2016).

3. Major Merger and Post-merger Stellar Mass Functions

In the following section, we present the stellar mass functions of local major mergers and post-mergers. We use these stellar mass functions to determine the major-merger fraction as a function of stellar mass. Furthermore, we determine the stellar mass functions of major mergers in different environments to compare our results to the predictions by P10.

3.1. Stellar Mass Functions of Major Mergers and Post-mergers

In Figure 2, we show the stellar mass functions of local major mergers and post-mergers based on the samples by D10 and Carpineti et al. (2012). As we discussed above, we combine three stellar mass function techniques according to Weigel et al. (2016). The results of the classical $1/V_{\rm max}$ and the SWML method are shown with open and filled symbols, respectively. The solid lines illustrate the results of the STY technique, and the shaded regions show the corresponding 1σ error contours. Upper limits are computed and shown for the $1/V_{\rm max}$ and SWML results. The best-fitting Schechter function parameters are given within the panels and are also given in Table 1, which summarizes the parameters of all stellar mass functions used in this analysis.

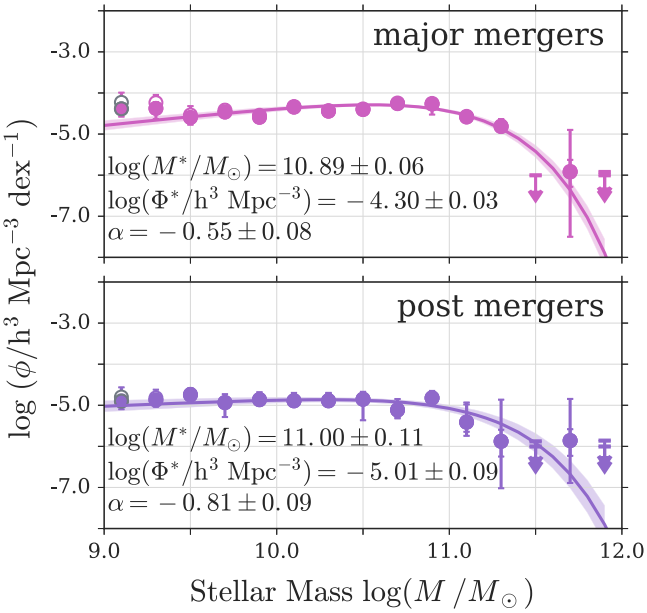

Figure 2. Stellar mass functions of local major mergers and post-mergers. To construct these stellar mass functions, we use the samples of visually classified major mergers and post-mergers by D10 and Carpineti et al. (2012), respectively. The open ($1/V_{\rm max}$) and filled (SWML) symbols and solid lines (STY) show the results of different stellar mass function techniques according to Weigel et al. (2016). Upper limits are computed based on both the $1/V_{\rm max}$ and SWML techniques. The best-fitting Schechter function parameters are given within the panels and are summarized in Table 1.

3.2. Merger Fraction

Having determined the stellar mass functions for major mergers and post-mergers, we are able to constrain the merger and post-merger fraction as a function of stellar mass. In the top panels of Figure 3, we compare the number densities of major mergers to the entire galaxy sample, all blue galaxies, and all red galaxies. The bottom panels illustrate the number density of post-mergers relative to the entire galaxy sample, all blue galaxies, and all red galaxies. At the bottom of each panel, we give the number of objects in each mass bin that was used to compute the stellar mass functions. The top and the bottom rows show the number of objects used for the numerator and the denominator, respectively.

We compare the major-merger fraction relative to all galaxies in our sample (top left-hand panel in Figure 3) to the results by D10. D10 report a major-merger fraction that ranges between 1.5% and 4.5%. This estimate is not based on the original major-merger catalog, which we use for our analysis, but on an extended sample of "strongly perturbed" galaxies in the local universe. D10 add expert visual assessments of galaxies with $f_{\rm m} < 0.4$ to derive the overall fraction of galaxies observed in a major merger. Furthermore, D10 introduce an absolute magnitude limit

Table 1
Best-fitting Schechter Function Parameters

Sample	S	D	Nr. objects	$\log(M^*/M_\odot)$	$\log(\Phi^*/h^3\,\mathrm{Mpc}^{-3})$	α	$\log(\Phi_2^*/h^3\,\mathrm{Mpc}^{-3})$	α_2	$\chi^2_{\mathrm{reduced}}$
Entire sample	⋯	X	69289	10.79 ± 0.01	-3.31 ± 0.20	-1.69 ± 0.10	-2.01 ± 0.28	-0.79 ± 0.04	9.78
Blue	X	⋯	32825	10.60 ± 0.01	-2.43 ± 0.01	-1.21 ± 0.01	⋯	⋯	4.70
Green	⋯	X	13429	10.65 ± 0.02	-3.95 ± 0.23	-1.84 ± 0.15	-2.54 ± 0.33	-0.44 ± 0.07	5.94
Red	⋯	X	26143	10.77 ± 0.01	-6.73 ± 0.79	-3.12 ± 0.51	-2.21 ± 1.12	-0.46 ± 0.02	6.67
Major mergers	X	⋯	276	10.89 ± 0.06	-4.30 ± 0.03	-0.55 ± 0.08	⋯	⋯	1.93
Post-mergers	X	⋯	104	11.00 ± 0.11	-5.01 ± 0.09	-0.81 ± 0.09	⋯	⋯	1.04
Early types & blue	X	⋯	219	10.66 ± 0.08	-4.47 ± 0.06	-0.72 ± 0.11	⋯	⋯	0.72
Early types & green	⋯	X	735	10.75 ± 0.05	-7.14 ± 1.12	-2.95 ± 0.71	-3.82 ± 1.57	-0.46 ± 0.16	0.74
Early types & red	⋯	X	8035	10.74 ± 0.01	-7.07 ± 0.80	-3.09 ± 0.57	-2.62 ± 1.14	0.13 ± 0.03	3.19
Major mergers & $\log(\delta+1) > 0.05$	⋯	X	216	10.77 ± 0.08	-7.76 ± 1.12	-2.99 ± 0.70	-4.25 ± 1.58	-0.14 ± 0.23	1.36
Major mergers & $\log(\delta+1) \leqslant 0.05$	X	⋯	68	10.90 ± 0.16	-5.25 ± 0.15	-0.92 ± 0.13	⋯	⋯	1.06
Mergers & satellites	X	⋯	134	10.94 ± 0.10	-4.70 ± 0.07	-0.69 ± 0.11	⋯	⋯	1.84
Mergers & centrals	X	⋯	161	10.90 ± 0.08	-4.56 ± 0.04	-0.53 ± 0.10	⋯	⋯	2.22

Note. We determine the parameters based on the parametric maximum likelihood approach (STY; Sandage et al. 1979) and give the 1σ random errors, which we compute directly from the STY MCMC chain. The second and third columns show whether the subsample is better described by a single (S) or by a double (D) Schechter function according to the likelihood ratio test, which we use to compare the STY single and double Schechter likelihoods. The number of objects given in the fourth column corresponds to the number of galaxies above the mass completeness cut. The $\chi^2_{\mathrm{reduced}}$ value given in the last column was derived by comparing the non-parametric maximum likelihood values (SWML; Efstathiou et al. 1988) to the STY best-fitting Schechter function.

($M_r < -20.55$) to construct a volume-complete sample. For our sample, the number of major mergers relative to all galaxies ranges from 0%–10% at a given stellar mass. There is no need to construct a volume-complete sample since we use stellar mass functions to measure the merger fraction, i.e., we correct for volume and stellar mass completeness effects. By integrating the merger fraction over M from $9 < \log(M/M_\odot) < 12$ (not including upper limits), we find a fraction of ∼2%. Note that our stellar mass functions show the number density of major-merger systems and not the number density of galaxies involved in a major merger. Assuming that on average each merger system contains two galaxies, the fraction of galaxies in a major merger relative to all galaxies is thus ∼4%, which is consistent with the results of D10.

Figure 3 shows an increase in the major-merger fraction relative to all blue galaxies toward higher masses. A similar, but weaker, trend can be seen for the number of major mergers relative to the entire galaxy sample and relative to red galaxies.

For simulations, this trend has been discussed by, for example, Bertone & Conselice (2009) and Hopkins et al. (2010a, 2010b). Hopkins et al. (2010a, 2010b) argue that while the halo merger fraction shows no strong halo mass dependence, it is the stellar mass to halo mass conversion (e.g., Behroozi et al. 2013) that introduces the stellar mass dependence in the galaxy merger fraction. At low halo masses, a 1:3 halo mass merger corresponds to a minor galaxy merger since the stellar mass to halo mass relation is steep, i.e., a small halo mass range corresponds to a wide stellar mass range. At high halo masses, even a minor halo mass merger corresponds to a major galaxy merger as the stellar mass to halo mass conversion is shallow, i.e., a wide range in halo mass corresponds to a small range in stellar mass. Compared to the halo major-merger fraction, the galaxy major-merger fraction is thus suppressed at low stellar masses and enhanced at high stellar masses.

Observational estimates of the merger fraction are method dependent (Lotz et al. 2011). Due to this, no clear consensus regarding the mass or luminosity dependence of the major-merger fraction has been reached. For example, Casteels et al. (2014) use morphological measurements based on concentration, asymmetry, and clumpiness (CAS) to identify major mergers. They find a merger fraction that is consistent with being constant at stellar masses $9.5 < \log(M/M_\odot) < 11.5$. This is in agreement with the results of Xu et al. (2012), who find a constant pair fraction for the same mass range. At stellar masses below $\log(M/M_\odot) = 9.5$, Casteels et al. (2014) find an increased merger fraction. Domingue et al. (2009) and Xu et al. (2004) find close pair fractions that are constant and increase with luminosity, respectively. At $z \sim 0.5$, Bundy et al. (2009) find a pair fraction that increases as a function of stellar mass.

3.3. Mass and Environment Quenching

In the following section, we compare the major-merger stellar mass function to the predictions by P10. We first summarize the results by P10 and then discuss the implications of our measurements.

3.3.1. The Empirical Model

In their purely empirical model, P10 consider three physical processes that are likely to lead to quenching and predict the corresponding stellar mass functions. The following three processes are the quenching channels that they consider:

1. *Mass Quenching*: mass quenching is independent of the environment, but does depend on stellar mass. Mass-quenched galaxies follow a single Schechter function. Compared to the mass function of blue galaxies, this Schechter function has the same M^*, but a shallower, more positive slope α ($M^*_{\mathrm{mass}} = M^*_{\mathrm{blue}}$, $\alpha_{\mathrm{mass}} = \alpha_{\mathrm{blue}} + 1$). Mass quenching could be associated with AGN feedback (Silk & Rees 1998; Di Matteo et al. 2005; Schawinski et al. 2006; Kauffmann et al. 2007; Georgakakis et al. 2008; Cattaneo et al. 2009; Hickox et al. 2009; Fabian 2012;

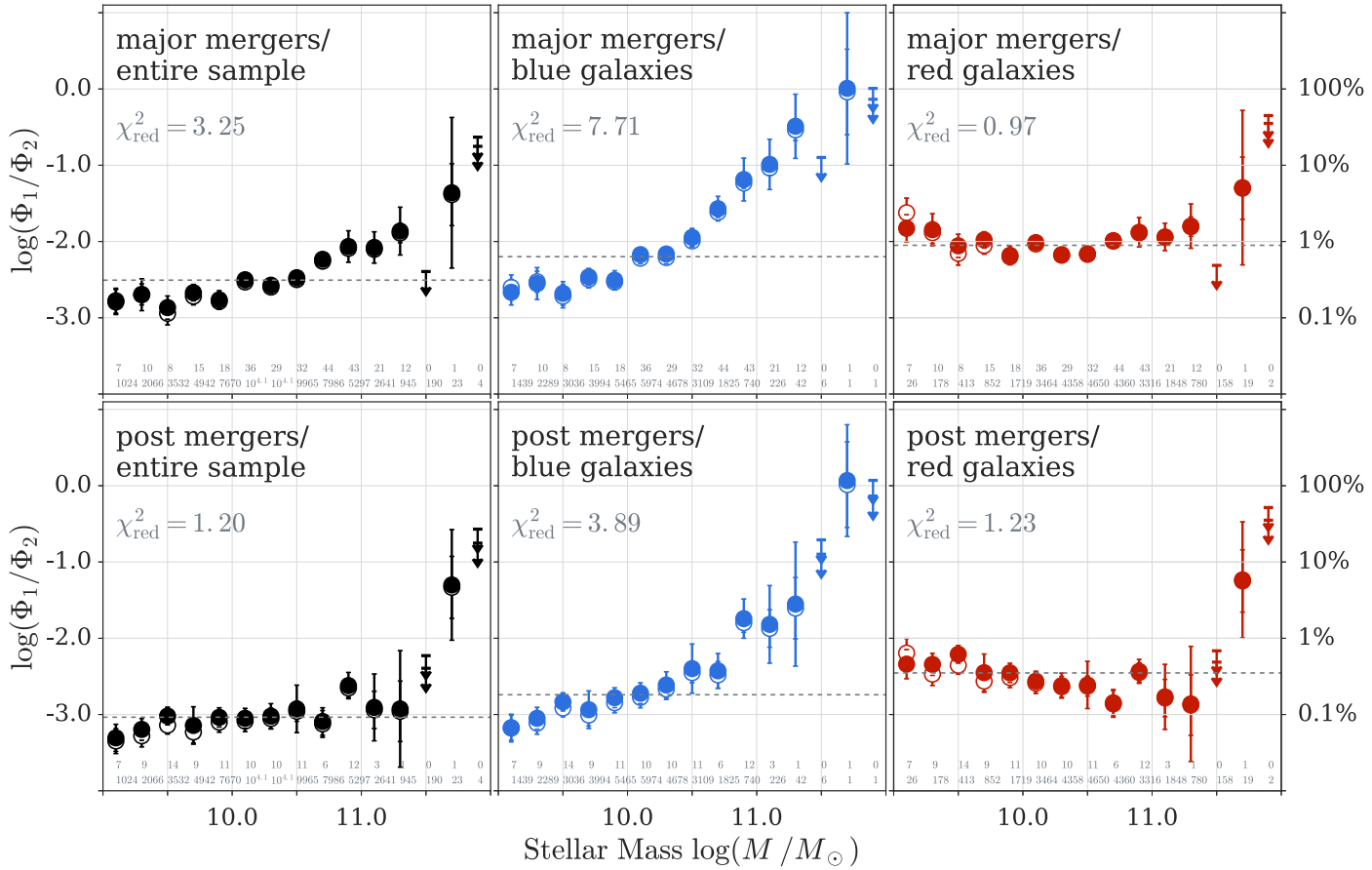

Figure 3. Merger fractions. The top panels show the number density of major mergers relative to the number density of all, all blue, and all red galaxies. The bottom panels show the number of post-mergers relative to the entire galaxy sample, all blue galaxies, and all red galaxies. In analogy to Figure 2, the open and filled markers show the fractions based on the $1/V_{\rm max}$ and SWML results, respectively. Upper limits are computed using the Φ values from both methods, which is why for some of the mass bins we show two upper limits. The gray dashed lines show the best-fitting relation for a constant fraction. The corresponding $\chi^2_{\rm reduced}$ values are given within the panels. The numbers at the bottom of the panels correspond to the number of galaxies in each mass bin that was used to compute the stellar mass functions. The top and the bottom rows show the number of objects used for the numerator and the denominator mass functions, respectively.

Bongiorno et al. 2016; Smethurst et al. 2016) or secular processes (Kormendy & Kennicutt 2004; Masters et al. 2011; Cheung et al. 2013).

2. *Satellite Quenching*: satellite quenching is mass independent, but environment dependent. As the satellite-quenching efficiency is mass independent, the stellar mass function of satellite-quenched galaxies has the same single Schechter function shape as blue, star-forming galaxies ($M^*_{\rm env} = M^*_{\rm blue}$, $\alpha_{\rm env} = \alpha_{\rm blue}$). Satellite quenching could be associated with external processes such as ram pressure stripping (Gunn & Gott 1972) or strangulation (Larson et al. 1980; Balogh et al. 2000).
3. *Merger Quenching*: merger quenching has the same properties as satellite quenching. P10 assume that the merger quenching efficiency is mass independent, but environment dependent. They thus predict the mass function of merger-quenched galaxies to have the same shape as the mass function of satellite-quenched galaxies.

The sum of mass-, satellite-, and merger-quenched galaxies makes up the red sequence, and the combination of their respective single Schechter functions reproduces the double Schechter function that we observe for red galaxies ($M^*_{\rm red} = M^*_{\rm blue}$, $\alpha_{1,\rm red} = \alpha_{\rm env}$, $\alpha_{2,\rm red} = \alpha_{\rm mass}$). We illustrate the effect of mass, satellite, and merger quenching in Figure 4.

As merger and satellite quenching have the same properties and result in the same stellar mass function shape, these two processes are often considered as one environment-dependent quenching channel. P10 argue that merger and satellite quenching are different manifestations of the same physical processes: a dark matter halo merger. If the baryonic galaxies merge, we observe a merger-quenched galaxy. If the baryonic galaxies do not merge, we conclude that satellite quenching has occurred. We refer to these two processes as environment quenching.

An important part of the P10 model is the fact that the quenching channels can be disentangled based on their environmental dependence. According to P10, satellite and merger quenching is dominant in overdense regions and mostly affects satellites. Mass quenching becomes apparent in underdense regions and mainly causes centrals to quench.

3.3.2. The Observations

We now compare our major-merger mass function to the predictions by P10. We not only consider the major-merger mass function, but also split the major-merger sample by environmental density to compare to the P10 predictions for different environments.

We determine the mass function of major mergers in over- and underdense regions (Weigel et al. 2016) and use the

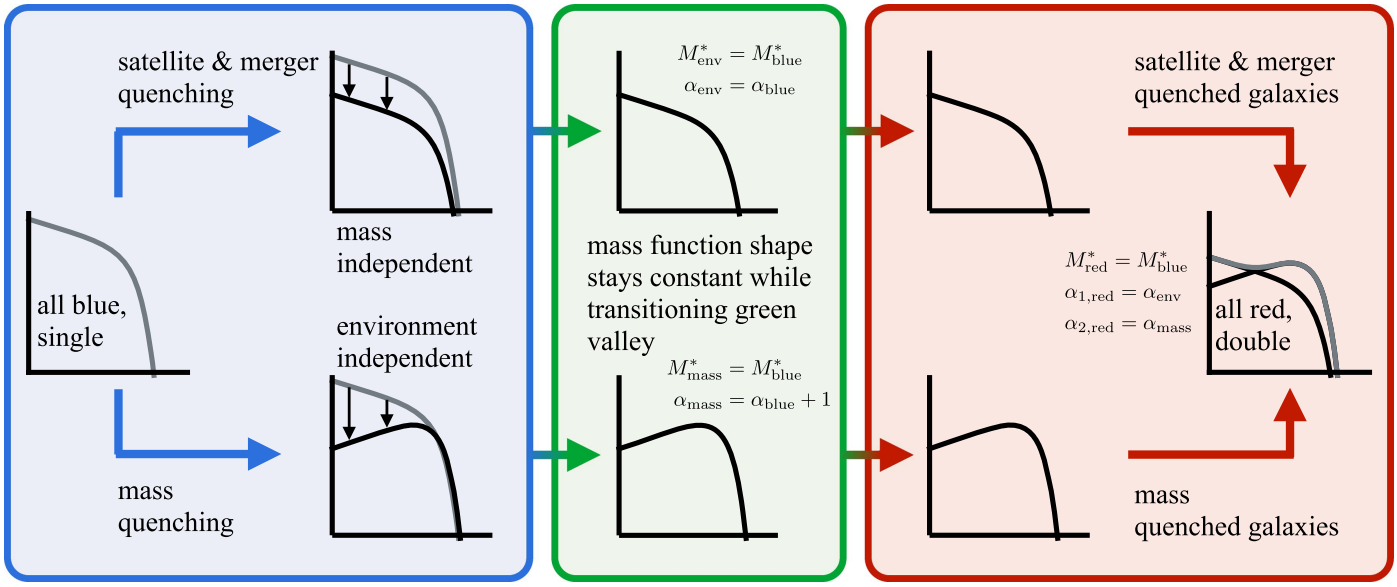

Figure 4. Schematic figure illustrating the phenomenological model by P10. In their model, P10 use three different quenching mechanisms to explain the double Schechter shape of the stellar mass function of red galaxies. *Mass quenching* (bottom row) is a mass-dependent, but environment-independent process. The cause of mass quenching is most likely an internal process, such as AGN feedback (e.g., Fabian 2012) or secular processes (e.g., Masters et al. 2011). The probability of a galaxy being mass quenched increases as a function of its stellar mass. P10 thus propose that when selecting blue galaxies that are in the process of being mass quenched, we will observe a stellar mass function that has the same M^* as blue galaxies, but a shallower slope α ($M^*_{\rm mass} = M^*_{\rm blue}$, $\alpha_{\rm mass} = \alpha_{\rm blue} + 1$). In the P10 model, *satellite* and *merger quenching* (top row) are processes that are mass independent, but environment dependent. According to P10 these processes are different manifestations of a dark matter halo merger. Galaxies that are being satellite or merger quenched have the shape of the blue, star-forming mass function ($M^*_{\rm env} = M^*_{\rm blue}$, $\alpha_{\rm env} = \alpha_{\rm blue}$). Leading to the same mass function shapes, these effects can thus be summarized as one environmental quenching process. While in transition, the green valley galaxies do not gain significant amounts of mass. The stellar mass functions hence retain their shapes. Mass-, merger-, and satellite-quenched galaxies make up the red sequence. The double-Schechter-shaped red mass function is the combination of the mass- and environment-quenched single Schechter mass functions ($M^*_{\rm red} = M^*_{\rm blue}$, $\alpha_{1,\rm red} = \alpha_{\rm env}$, $\alpha_{2,\rm red} = \alpha_{\rm mass}$).

central/satellite classification by Yang et al. (2007) to split the major-merger sample into centrals and satellites. Note that this does not imply that we are generating the mass functions of major satellite−satellite or major central−central mergers. Instead, we determine whether the galaxies that we are considering in the construction of the major merger mass function are classified as a satellite or as a central (see Section 2.3).

We show the stellar mass functions for major mergers, major mergers in over- and underdense regions, and the mass functions of central and satellite major mergers in Figure 5. Overplotted with dashed and dotted lines, we illustrate the shape that we would expect to see for mass and environment quenching, respectively. Note that P10 only predict the shape and not the normalization of the mass and environment quenching mass functions. For an easier comparison, we thus rescale the predicted mass functions to match the Φ^* of the subsample that we are considering.

First, let us consider the general major merger mass function shown in the upper left-hand panel of Figure 5. According to the P10 model, merger quenching is an environment-dependent effect. The mass function of merger-quenched galaxies should thus have the same shape as the blue mass function, indicated by the blue dotted line in Figure 5. Contrary to the prediction by P10, the observed major-merger mass function is however consistent with the mass quenching mass function.

We find a similar inconsistency if we split the major-merger sample by overdensity. The observed stellar mass functions for mergers in over- and underdense regions are shown in the upper middle and right-hand panels, respectively. The mass function of mergers in overdense regions resembles neither the mass nor the environment quenching mass function. In underdense regions, mass quenching effects should be dominant. Yet the observed merger mass function has an M^* that is too high to be consistent with the environment quenching mass function and is too flat to follow the mass quenching mass function.

The mass function of central major mergers, shown in the bottom right-hand panel, is the only case where our observations match the expectations. As predicted, the mass function of central major mergers is consistent with the mass quenching mass function. The mass function of satellite major mergers does, however, also resemble the mass quenching mass function, even though environmental quenching effects should dominate. This is shown in the middle panel at the bottom.

We conclude that our measurement of the major-merger mass function is inconsistent with the empirical model by P10. Besides the major-merger mass functions, there are additional indicators of the P10 model being oversimplified with respect to merger quenching. A fundamental assumption of the model is the fact that the mass functions of red and blue galaxies have the same M^*. However, for our sample, $M^*_{\rm red} - M^*_{\rm blue} \sim 0.2$ dex (see Table 1 Weigel et al. 2016). Furthermore, P10 assume a mass-independent merger quenching efficiency. Contrary to this assumption, we find a mass-dependent merger fraction, as we discussed in Section 3.2 and show in Figure 3. P10 also assume that the merger quenching efficiency increases as a function of environmental density. Yet in massive systems such as clusters, galaxies have high relative velocities, and the probability of mergers is expected to decrease (Ostriker 1980).

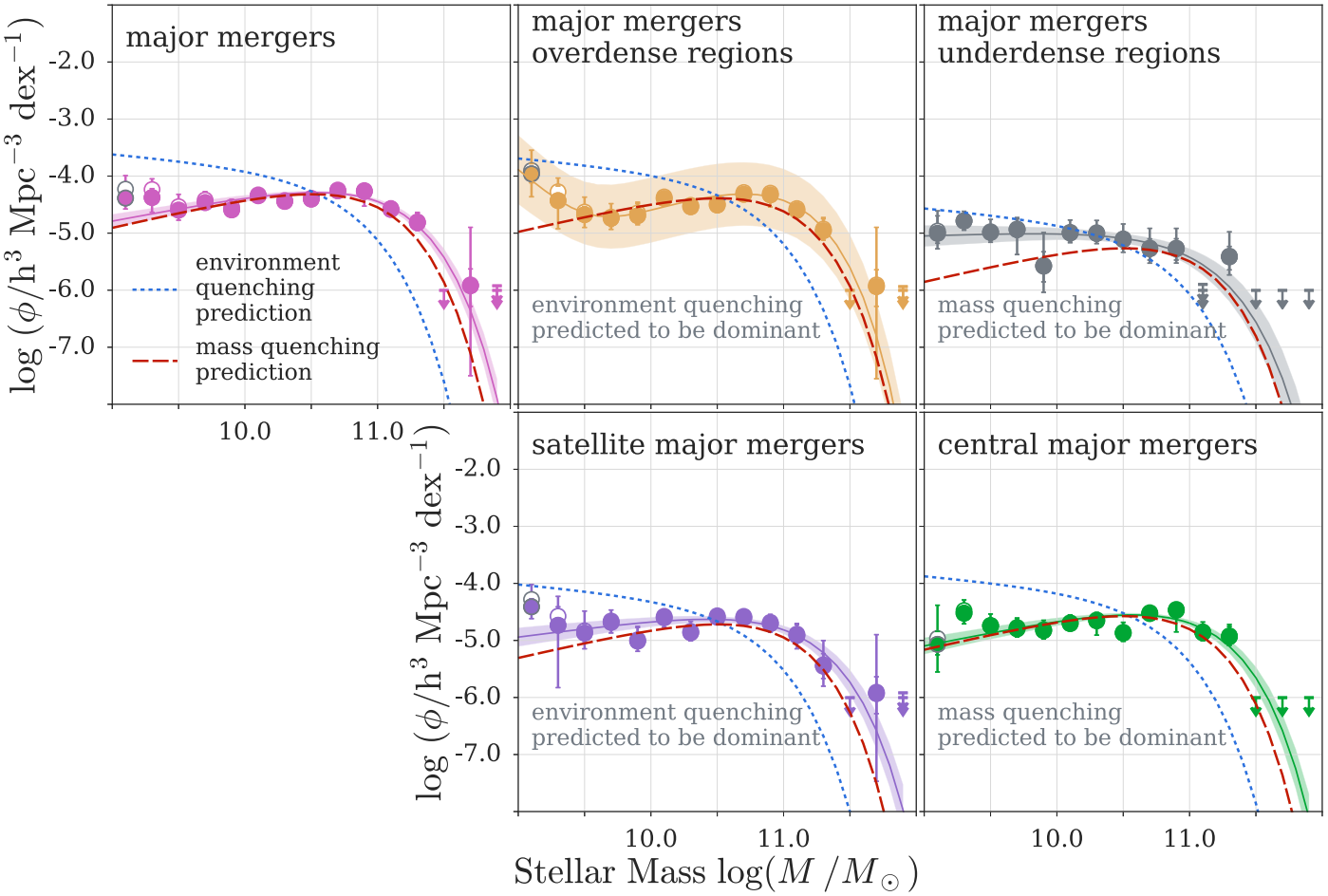

Figure 5. Stellar mass functions for major mergers, major mergers in overdense and underdense regions, and satellite and central major mergers. An important part of the empirical P10 model is the fact that mass- and environment-dependent quenching mechanisms can be disentangled by considering over- and underdense regions. Environment quenching is dominant in overdense regions and mostly affects satellites. Mass quenching becomes apparent in underdense regions and primarily quenches centrals. We split the major-merger sample by density (Weigel et al. 2016) and into centrals and satellites (Yang et al. 2007) to test whether the major-merger mass function is consistent with the P10 model. From top left to bottom right, we show the stellar mass functions of all major mergers, mergers in overdense and underdense regions, and satellite and central major mergers. Overplotted in red and blue are the predictions for mass and environment quenching according to the P10 model. To allow for an easier comparison, the predicted mass functions are rescaled to have the same Φ^* as the observed ones. In the P10 model, merger quenching is an environment-dependent, but mass-independent, process. The observed mass function of all major mergers (top left-hand plot) should thus resemble the predicted environment quenching mass function (blue dotted line). However, contrary to the P10 prediction, the merger mass function shape is consistent with the mass quenching mass function. The shapes of the observed merger mass functions in over- and underdense regions match neither the predicted mass nor environment quenching mass function. As predicted by P10, the observed mass function of central major mergers is consistent with the predicted mass quenching mass function. For satellite major mergers, environmental quenching effects should be dominant. However, the slope α of the observed satellite major-merger mass function is too shallow to be consistent with environment quenching. This figure thus illustrates that our observations of the merger quenching process in the local universe are inconsistent with the empirical model by P10.

4. Major Mergers as a Quenching Mechanism—Model

4.1. Assumptions and Expectations

We now use the local major-merger and post-merger mass functions to investigate the process of major-merger quenching. To do so, we make the following straightforward assumptions:

1. galaxies that are in the process of being major-merger quenched evolve along the following sequence of stages, which we refer to as the "merger quenching sequence": major merger, post merger, blue early type, green early type, red early type;
2. the probability of galaxies evolving from the major-merger to the red early-type stage is mass independent;
3. while transitioning, the population of merger-quenched galaxies does not increase its stellar mass significantly, thereby retaining its mass distribution.

These assumptions imply that the stellar mass functions of major mergers, post-mergers, blue early types, green early types, and red early types are similar in shape. They allow us to investigate:

1. if major mergers are likely to lead to quenching,
2. the relative amount of time spent in stages along the merger quenching sequence,
3. and the significance of major-merger quenching.

In the following section, we give the motives for our assumptions. We discuss the merger quenching sequence and the order of its stages, the mass dependence of the major merger to red early-type transition probability, and the possible increase in stellar mass along the sequence. In Section 5, we apply these assumptions to our sample and use them to investigate major-merger quenching.

4.2. Major-merger Quenching Stages and Their Order

We focus on mergers between gas-rich galaxies of comparable mass (mass ratio 1:3 and greater). According to Toomre & Toomre (1972), these major mergers are capable of transforming disk galaxies into spheroids or ellipticals, which has now also been shown and studied in various simulations (e.g., Mihos & Hernquist 1996; Di Matteo et al. 2005; Springel et al. 2005a; Croton et al. 2006; Hopkins et al. 2006, 2008a, 2008b; Khalatyan et al. 2008; Somerville et al. 2008). Furthermore, previous studies have investigated the evolution of merging galaxies both in terms of color (e.g., Kaviraj et al. 2011) and SFR (e.g., Springel et al. 2005a; Hopkins et al. 2008b). Based on these studies, we assume that galaxies that evolve along the classical Sanders et al. (1988) quenching sequence are likely to pass through the following stages:

1. *Major-merger Stage:* we base our analysis on the Galaxy Zoo major-merger sample (D10; Darg et al. 2010b), which contains visually classified merger systems. These systems consist of at least two strongly perturbed, close-by galaxies. Disrupted tidal fields and dynamical friction drive the merging galaxies toward each other, and violent relaxation rearranges the stellar orbits (Bournaud 2011).
2. *Post-merger Stage:* after coalescence, only one nucleus remains, and the galaxy is likely to have a disturbed morphology—it might, for example, be exhibiting tidal tails. Gravitational torques cause angular momentum loss and allow the gas to fall toward the center of the newly formed galaxy (Hernquist 1989; Mihos & Hernquist 1996; Carpineti et al. 2012). The high central gas densities trigger a starburst and an AGN. Due to the large amounts of gas and dust, the galaxy is classified as an ultraluminous infrared galaxy (ULIRG; Sanders & Mirabel 1996; Genzel et al. 2001).
3. *Blue Early-type Stage:* the galaxy has now lost its signs of a recent major merger (see discussion below) and appears to have an early-type morphology. Kinetic and thermal feedback from the AGN and/or from supernovae expel or heat the gas in the galaxy, thereby quenching star formation (Kaviraj et al. 2007). This has been predicted theoretically (Di Matteo et al. 2005; Springel et al. 2005b; Croton et al. 2006; Khalatyan et al. 2008; Somerville et al. 2008) and confirmed observationally (Schawinski et al. 2006; Tremonti et al. 2007; Schawinski et al. 2007; Wong et al. 2015, but also see: Ellison et al. 2015; French et al. 2015).
4. *Green Early-type Stage:* as the SFR declines, the galaxy transitions through the green valley. Showing signs of recent star formation, the galaxy is classified as a post-starburst galaxy (PSG/E+A/K+A; Bekki et al. 2001; Goto 2005; Yamauchi et al. 2008; Wong et al. 2012). This stage can also be accompanied by AGN activity (Yan et al. 2006).
5. *Red Early-type Stage:* once the remaining gas is consumed, the galaxy reddens and reaches the red sequence as a red early-type galaxy.

The sequence that we set out above consists of dividing the entire galaxy sample both in terms of morphology and color. First, we use visual morphologies to select major mergers, post-mergers, and early types. Second, we use the optical color as a proxy for SFR to select early types in the blue cloud, green valley, and red sequence. This allows us to trace the shutdown of star formation in these merger remnants.

Along the sequence, galaxies transition from the post-merger to the blue early-type stage. We thus seem to assume that the change in morphology precedes the change in color. This seems to imply that the dynamical or the relaxation timescale of merger remnants is shorter than the duration of their starbursts. Yet it is important to consider the data to which we will be applying this model. Specifically, the selection of early-type galaxies has to be taken into account.

In Section 5, we will apply our assumptions to a sample of galaxies that have been classified by Galaxy Zoo users. Users were asked to classify galaxies according to their SDSS images. Schawinski et al. (2010) use a sample of blue early-type galaxies with SDSS classifications (Schawinski et al. 2007) to show that at least 50% of all blue early types show signs of a recent merger in co-added Stripe 82 images. These images are approximately two magnitudes deeper than regular SDSS images. Similarly, van Dokkum (2005) uses deep imaging ($\sim$28 mag arcsec^{-2}) from the Multi-wavelength Survey by Yale-Chile (MUSYC; Gawiser et al. 2006) and the NOAO Deep Wide-Field Survey (NDWFS; Jannuzi & Dey 1999) and finds that 53% of the nearby, red galaxies in the sample show signs of tidal interactions. When restricting the sample to bulge-dominated early-type galaxies, this fraction increases to 71%. We are thus not proposing that merger remnants have lost all signs of recent mergers and are fully relaxed by the time they leave the blue cloud. Instead, we assume that the low surface brightness tidal features have faded and are no longer visible in the shallow SDSS images. Missing the signs of morphological disturbance, the still-blue merger remnants are classified as early types.

We also note that AGN activity has been found to peak during different stages along the merger quenching sequence (Koss et al. 2010; Schawinski et al. 2010; Ellison et al. 2011, 2013; Carpineti et al. 2012, 2015; Kaviraj et al. 2015). As we discussed above, the definition of the post-merger and blue early-type stage depends on the specifics of the sample and the method used to select, for instance, post-merger galaxies. It is thus difficult to directly compare previous studies. In the sequence that we set out above, black holes increase their accretion rate during the post-merger stage and provide the necessary feedback for a decrease in SFR in the blue early-type stage. The result of AGN and star formation feedback becomes apparent during the green early-type stage, once the galaxy has significantly decreased its SFR. However, we cannot determine the exact time during the evolution in which galaxies have experienced sufficient feedback to quench their star formation.

4.3. Mass Dependence of the Transition Probability

Below we discuss three processes that could cause the probability of a galaxy to transition from the major-merger to the red early-type stage to be mass dependent. As stated above, we assume that these effects are negligible and do not introduce a significant mass dependence in the space density of galaxies that are being major-merger quenched.

1. *Reforming of a Disk:* simulations have shown that, unlike the sequence that we laid out above, a major merger between two spiral galaxies of comparable mass can also lead to the formation of a new spiral galaxy (Hernquist & Barnes 1991; Barnes & Hernquist 1996; Barnes 2002; Naab et al. 2006; Robertson & Bullock 2008). In most models, the probability of reforming a disk depends on

the gas fraction within the merging galaxies and the amount of stellar or AGN feedback during the merger. Other parameters such as the mass ratio of the merging galaxies, their orbital parameters, and their mass distributions also affect the probability of regrowing a disk (see, e.g., Hopkins et al. 2009). The high gas fractions that are necessary for a merger remnant to be able to regrow its disk are typically found in galaxies at $z > 1$ (Daddi et al. 2010; Tacconi et al. 2010). In the model by Robertson et al. (2006), the gas fraction has to be above 50% for a disk to reform. Springel & Hernquist (2005) use pure gas disks to model the reformation of a rotationally supported disk after the merger. In the model by Governato et al. (2009), the merging galaxies have a gas fraction below 25% at $z < 3$, yet the simulation involves the constant accretion of gas through cold streams and efficient gas cooling.

Observationally, the regrowing of a disk in a post-merger galaxy has been observed in the local universe (see e.g., Hau et al. 2008; Kannappan et al. 2009; Moffett et al. 2012; Salim et al. 2012; Ueda et al. 2014; George 2017). Blue early-type galaxies with signs of a disk seem to primarily occur in low-mass galaxies (e.g., $<3 \times 10^{10}\,M_{\odot}$; Kannappan et al. 2009). Compared to more massive galaxies, the regrowing of a disk after a major-merger event in lower mass galaxies could be promoted by higher gas fractions (Catinella et al. 2010).

The regrowing of a disk after a major-merger event is hence theoretically possible and has been observed for a small sample of local galaxies. Yet the significance of this effect on the mass dependence of the merger quenching probability remains unclear. Robust to a mild mass dependence, the mass functions of galaxies along the merger quenching sequence would however only be affected if this were a strongly mass-dependent effect. For instance, if $10^9\,M_{\odot}$ galaxies are more than 50% more likely to regrow a disk than M^* galaxies, the resulting difference in the space densities at these masses would affect the α of the resulting mass function. We make the simplified assumption that such an extreme effect is unlikely and neglect the process of disk reforming on the transition probability.

2. *AGN Feedback:* AGN feedback is necessary to efficiently quench a merger remnant (Springel et al. 2005a; Birnboim et al. 2007; Hopkins et al. 2008b; Khalatyan et al. 2008). Without AGN feedback, a merger remnant can return to being a star-forming late type (Sparre & Springel 2016). Furthermore, AGN feedback has to be introduced to explain the high gas depletion rate and the rapid early-type evolution (Schawinski et al. 2014; Smethurst et al. 2016) from blue to red (Kaviraj et al. 2011). Recent work has shown that observed AGN luminosity functions are consistent with a mass-independent AGN fraction and accretion rate distribution (Aird et al. 2012, Weigel et al. 2017). We thus assume that the probability of a merger remnant being affected by sufficient AGN feedback to transition to the red sequence is mass independent.
3. *Dynamical Friction*: Chandrasekhar (1943) introduced the concept of dynamical friction being mass dependent. More recently, Jiang et al. (2008; also see Jiang et al. 2010) have shown that the resulting mass dependence of the merger timescale is best expressed as $T \propto M_{\rm primary}/(M_{\rm secondary} \times \ln(1 + M_{\rm primary}/M_{\rm secondary}))$. Here, $M_{\rm primary}$ and $M_{\rm secondary}$ refer to the more massive and less massive merging partners, respectively. Given our major merger definition, this causes up to a factor of 1.5 difference in the merging timescale of merging systems depending on their mass ratio. Jiang et al. (2008) consider the time between the secondary first crossing the dark matter virial radius of the primary and the beginning of the coalescence as their merging time. We assume that the galaxies in the D10 sample, which show clear signs of interaction, are close to coalescence and neglect the mass ratio and thus mass dependence of dynamical friction.
4. *Fading of Merger Features:* as we discussed above, we assume that the post-merger stage is followed by the blue early-type stage, as for most galaxies the signs of a recent merger will have faded enough to no longer be detected in the shallow SDSS images. We assume that there is no mass dependence in the timescale over which these tidal features fade. There might be galaxies for which the signs of a recent merger fade less quickly and which might be classified as post-mergers instead of, for instance, green early types. However, if mass independent, this effect does not introduce a bias in the space density of galaxies that we observe along the merger quenching sequence.

4.4. Mass Increase along the Quenching Sequence

During their evolution from blue to red, merger-quenched galaxies can gain stellar mass through three different channels:

1. *Through Star Formation:* while transitioning from the blue cloud to the red sequence, a galaxy retains low levels of SFR. However, even if a galaxy would keep its pre-quenching SFR, the amount of gained stellar mass would be negligible compared to the galaxy's already existing stellar mass. For example, a M^* galaxy of $10^{10.8}\,M_{\odot}$ (Weigel et al. 2016) has an SFR of $\sim 5\,M_{\odot}\ {\rm yr}^{-1}$ (Lilly et al. 2013) if it is on the main sequence. For a constant SFR, this galaxy will increase its stellar mass by a factor of 1.4 within 5 Gyr. So, even if the SFR were to stay constant during the transition from blue to red, the galaxy would only increase its stellar mass by 0.1 dex if the transition takes $\sim$5 Gyr.
2. *Through a Starburst During the ULIRG Phase:* as we mentioned above, a major-merger-quenched galaxy is likely to experience a starburst while transitioning from blue to red. Yet, similar to the argument in the first point, the galaxy will not gain significant amounts of stellar mass during the starburst phase (see, e.g., Genzel et al. 1998; Carpineti et al. 2015). Di Matteo et al. (2008), for instance, find that strong starbursts are rare in the local universe and that a merger-triggered starburst results in an SFR that is enhanced by less than a factor of five. They also find a typical starburst duration of the order of 10^8 years. For a M^* galaxy on the main sequence, this implies a $<$0.02 dex increase in stellar mass.
3. *Through the Mass of the Merging Partner:* through merging, a galaxy can increase its stellar mass by 0.3 dex at most. Assume we consider the blue spiral galaxy M_1 in our major-merger mass function construction. The galaxy M_1 is merging with, M_2, must have $M_2 \leqslant M_1$, otherwise we would have considered M_2 when

determining the stellar mass function. M_1's mass increases by 0.3 dex if $M_1 = M_2$. Mergers with low mass ratios are more common than mergers between galaxies of comparable mass (Kaviraj 2014). The number of galaxies that double their stellar mass, i.e., increase their mass by 0.3 dex, is thus likely to be low.

While transitioning from blue to red, galaxies are thus unlikely to gain significant amounts of mass. We expect galaxies in evolutionary stages between the blue cloud and the red sequence to have mass functions of the same shape if the transition probability is mass independent. The stellar mass function normalizations are expected to be the same if all galaxies spend the same amount of time in each stage and if all galaxies transition from one stage to the next. The mass function of the blue, still star-forming galaxies has a different normalization since galaxies spend a certain amount of time in this stage before the cessation of their star formation. The same is true for the mass function of the red and dead galaxies since this is the end stage and galaxies will accumulate here. The shape of the red mass function is the same as that of the transitioning objects, if the quenching process we are considering is the only way to build up a red galaxy and there are no other quenching channels. If galaxies spend less time in a certain stage or only a fraction of galaxies has transitioned from the previous stage, Φ^* of this stage decreases. The shape of the mass function of one of the phases changes if the transition from the previous stage is mass dependent and, for example, more efficient at higher stellar masses.

5. Major Mergers as a Quenching Mechanism—Analysis

Based on the assumptions that we introduced in the previous section, we now investigate the effect of quenching through major mergers in the local universe. We introduce the stellar mass functions of galaxies along the merger quenching sequence and test if they are similar in shape. We then use these stellar mass functions to estimate the relative amount of time that galaxies spent in stages along the sequence. To determine the significance of major-merger quenching, we introduce four tests that vary in their level of sophistication and assumptions. First, we compare the shapes of the major-merger and the red early-type mass functions. Second, we compare the major merger to the mass function of all green galaxies. Third, we estimate the contribution of major-merger-quenched galaxies to the green valley flux. Fourth, we simulate the evolution of the red stellar mass function and determine the fraction of galaxies that are likely to have been major-merger quenched within the last 5 Gyr. We end this section by summarizing our results regarding the significance of major-merger quenching.

5.1. Major-merger Quenching Sequence Mass Functions

Besides the stellar mass functions of major merger and post-mergers, which we introduced in Section 3.1, we also determine the mass functions of blue early types, green early types, and red early types. Figure 6 summarizes the stellar mass functions of all five merger quenching sequence stages. For comparison, we also show the stellar mass function of the entire galaxy sample in gray. In analogy to Figure 2, open ($1/V_{\rm max}$) and filled (SWML) symbols and solid lines (STY) show the results of the different stellar mass function estimators. For $1/V_{\rm max}$ and SWML, we show upper limits in stellar mass bins that do not contain any sources. The best-fitting STY Schechter function parameters and their errors are given in Table 1. Figure 7 summarizes and illustrates the major-merger quenching sequence.

As we have discussed above, based on our assumptions, we expect the stellar mass functions of galaxies along the quenching sequence to have similar shapes if none of the transitions is mass dependent. To test if this is the case for the mass functions that we are considering here and to make a possible mass dependence more apparent, we take the ratio between mass functions of consecutive steps along the quenching sequence. We refer to these ratios as "transition curves" and illustrate them in Figure 8.

From top left to bottom right, we show the transition curves for the major-merger to post-merger, the post-merger to blue early-type, the blue early-type to green early-type, and the green early-type to red early-type stages. For stellar mass functions of similar shapes, these transition curves are flat. Their normalization corresponds to the fraction of galaxies transitioning from one phase to the next, if we assume that the galaxies spend the same amount of time in each stage.

To quantify the flatness of the transition curves, we compute the $\chi^2_{\rm reduced}$ values for constant fractions. The $\chi^2_{\rm reduced}$ values are given within Figure 8. Note that for the $\chi^2_{\rm reduced}$ computation we use the SWML data points, and we do not take upper and lower limits into account. Based on the $\chi^2_{\rm reduced}$ values, Figure 8 shows that the transition curves of most stages are consistent with being flat, only the evolution from the green to the red early-type stage shows a significant mass dependence.

According to the STY method and the likelihood ratio test, the green early-type and the red early-type mass functions are well described by double Schechter functions. Compared to the green early types, the red early types are however fit by a stronger double Schechter with higher $\log(\Phi^*_2/\Phi^*_1)$ and α_2 values (see Figure 6 and Table 1). The red early types thus have a higher number density at high stellar masses, which causes the strong mass dependence that we see in the bottom-left panel of Figure 8. We discuss the implications of the green and the red early types having significantly different mass functions in more detail in Section 5.3.

We conclude that except for the evolution of green to red early types, the transition curves are consistent with being flat. We thus infer that the galaxies that we find in these different phases today are likely to evolve along a sequence. This sequence bridges the blue cloud to the red sequence, and does not include a significant mass dependence. Hence, major mergers are likely to lead to quenching for a majority of galaxies that are involved in a gas-rich merging event.

Our expectation of similar mass function shapes for galaxies along the merger quenching sequence is based on the assumption of a mass-independent merger-to-red-early-type transition probability. As we argued in Section 4.3, we assume that the effects of disk reforming, AGN feedback, dynamical friction, and fading of merger features do not introduce a significant mass dependence in the probability of a merger remnant reaching the red sequence. Implicitly, we also assume that the stellar mass measurements of major mergers and post-mergers and their visual classifications are unbiased. The transition curves of galaxies along the merger quenching sequence being flat thus either implies that our assumptions are

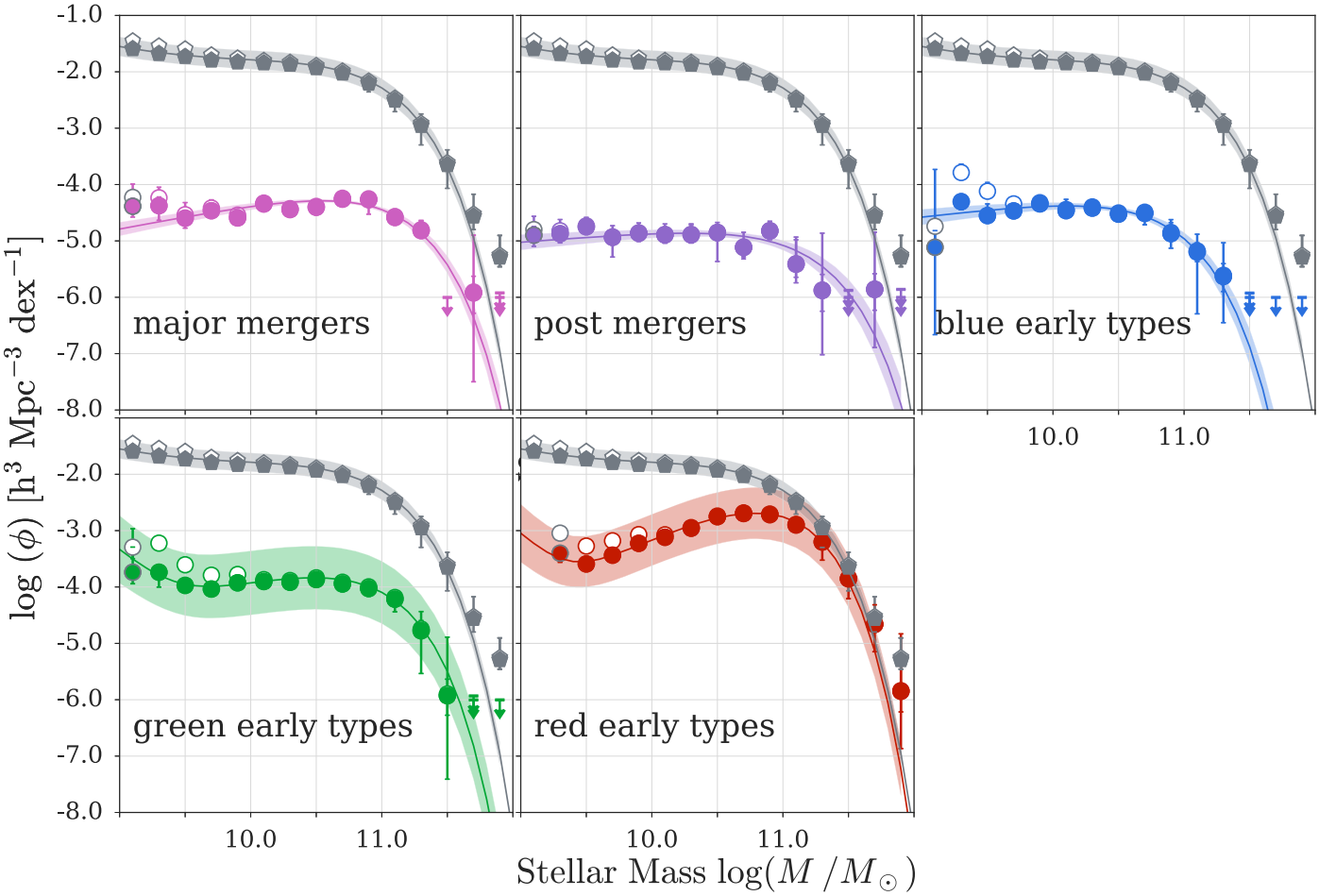

Figure 6. Stellar mass functions for major mergers, post-mergers, blue early types, green early types, and red early types. Shown in gray is the mass function of the entire galaxy sample. Results from the classical $1/V_{\rm max}$ approach (Schmidt 1968) and the non-parametric maximum likelihood technique (SWML; Efstathiou et al. 1988) are shown with open and filled symbols, respectively. The best-fit Schechter functions according to the parametric maximum likelihood approach (STY; Sandage et al. 1979) are illustrated with solid lines. The STY parameters of each subsample are given in Table 1. The shaded region shows the 1σ uncertainty according to the STY technique. The error bars on the $1/V_{\rm max}$ results correspond to the 1σ random error. The error bars on the SWML points show the combination of random errors and the systematic error due to stellar mass uncertainties. For stellar mass bins that do not contain any sources, we compute upper limits with the $1/V_{\rm max}$ and SWML method. Upper limits are computed for the SWML and $1/V_{\rm max}$ results, which is why for some of the mass bins, we show two upper limits. See Weigel et al. (2016) for more details.

justified or that two or multiple effects compensate for their respective mass dependence.

If there are, for instance, two mass-dependent mechanisms that have the opposite effect on the space density of merger-quenched galaxies, then they have to both affect the *same* stages along the merger quenching sequence. For example, if low-mass galaxies have a high probability of reforming a disk, we would expect these galaxies to be part of the major merger, but maybe not the green early-type sample. The space density of low-mass green early types would be lower, causing the green early-type mass function to have a different slope α from the major-merger mass function. This effect could not be compensated for by a mass dependence of dynamical friction, which would primarily affect major-merger and post-merger galaxies. Similarly, a systematic bias could affect the stellar mass measurements of major-merger and post-merger galaxies. Yet, we do not expect the stellar mass measurements of standard ellipticals to be affected by biases. The blue early-type mass function being similar in shape to the major-merger and post-merger mass functions hence provides evidence against a bias in the M measurement of major mergers and post-mergers, if we assume that the aforementioned effects are indeed mass independent.

We conclude that the probability of a mass dependence of the effects considered here causing mass functions of similar shapes for all stages along the merger quenching sequence is low. The simpler and more straightforward explanation for the flat transition curves shown in Figure 8 is that these stages do indeed represent an evolutionary sequence and that the previously mentioned effects do not significantly impact the mass distribution of galaxies following this evolution.

5.2. Transition Timescales

By assuming that along the major-merger sequence most galaxies transition from one phase to the next, we can constrain the relative amount of time spent in each phase. We consider the number density of galaxies in the major-merger, post-merger, blue early-type, and green early-type stages. We do not take galaxies in the red early-type phase into account since all quenched galaxies accumulate in this stage. We use the SWML results and calculate the relative amount of time spent in phase i

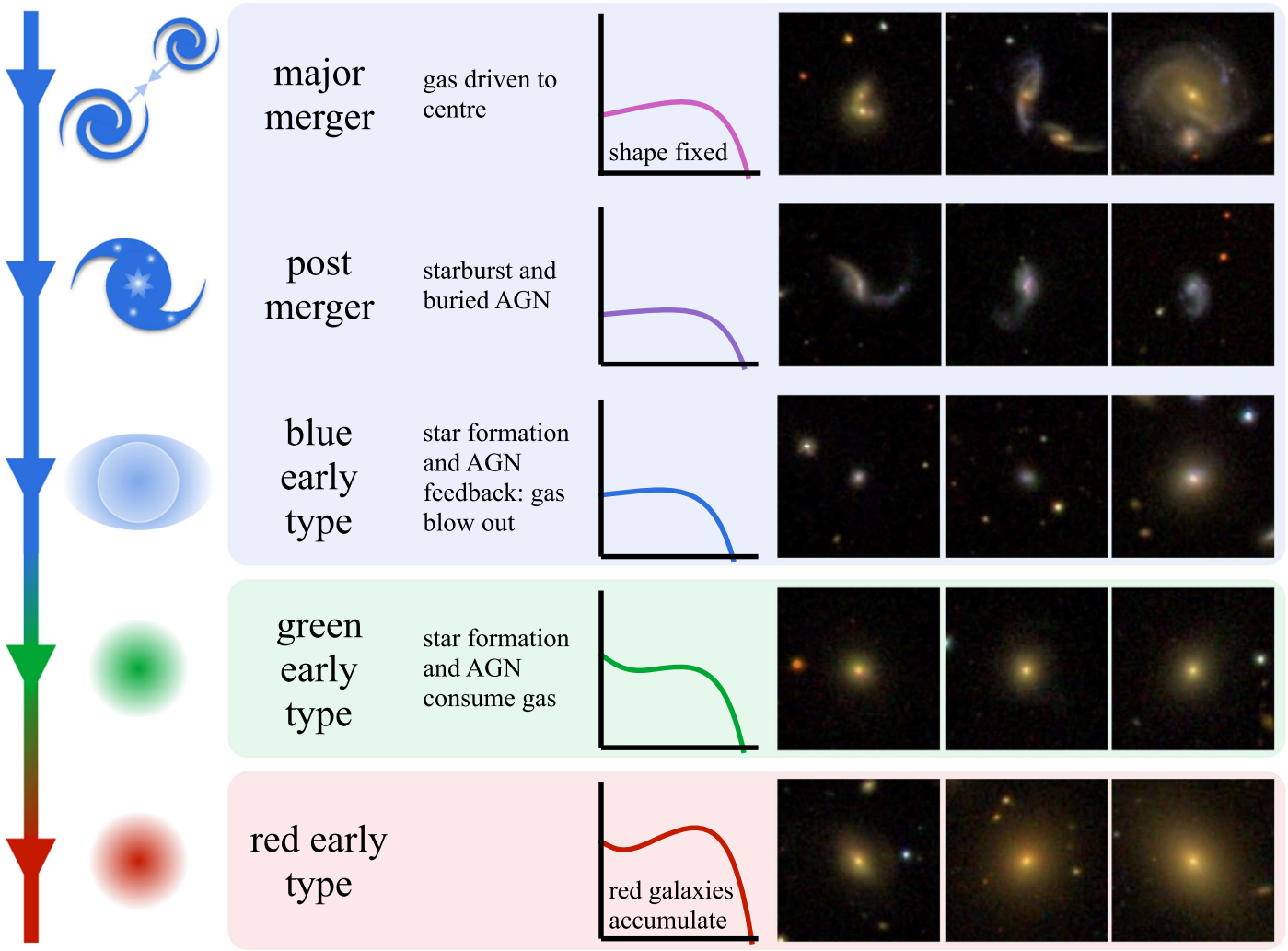

Figure 7. Schematic figure illustrating the process of major-merger quenching. We highlight the five main stages that we would expect a major-merger-quenched galaxy to pass through and show the corresponding stellar mass functions and SDSS example images. Note that the stellar mass functions illustrated here are a simplified version of the measured mass functions, which we show in Figure 6. All galaxy samples used here are based on visual classifications from Galaxy Zoo volunteers (Lintott et al. 2008, 2011). The main difference between the major-merger and the post-merger sample is the number of nuclei: major mergers contain at least two, whereas post-mergers only show one nucleus (Carpineti et al. 2012, D10, Darg et al. 2010b). As we discuss in more detail in the text, a merger between galaxies of comparable mass leads to the gas falling toward the center of the merger remnant. This can ignite both a starburst and an AGN. Their feedback can lead to quenching and an evolution of the merger remnant from the blue cloud to the red sequence. We use the stellar mass functions of galaxies along this quenching pathway to study the process of major-merger quenching and to estimate its significance.

for the mass bin k in the following way:

$$t_i(M_k) = \frac{\Phi_i(M_k)}{\sum_j^{N_{\rm states}} \Phi_j(M_k)}. \quad (5)$$

The 1σ error on t_i is given by

$$\sigma_{t_i}^2 = \sum_j^{N_{\rm states}} \left(\frac{\partial(\Phi_i/\sum\Phi)}{\partial\Phi_j} \right)^2 \sigma_{\Phi_j}^2 = \frac{1}{\left(\sum\Phi\right)^2} \left(\sum_j^{N_{\rm states}} \left(\frac{\Phi_j^2 \sigma_{\Phi_j}^2}{\left(\sum\Phi\right)^2} \right) + \left(1 - 2\frac{\Phi_i}{\sum\Phi} \right) \sigma_{\Phi_i}^2 \right). \quad (6)$$

Figure 9 summarizes our results and shows that at a given stellar mass, galaxies spend ~60% of their transition time in the green early-type stage. The post-merger sample contains only very few galaxies. This implies that galaxies spend only ~5% of their time in the post-merger stage.

The numbers at the bottom of Figure 9 show the number of objects in each mass bin that were used to compute the stellar mass functions of the samples used here (from top to bottom: green early types, major mergers, blue early types, post-mergers). Due to the low number density of high-mass galaxies, our sample contains only very few galaxies at masses above $\log(M/M_\odot) = 11.3$. For example, the $\log(M/M_\odot) = 11.5$ mass bin only contains one green early-type and no major merger, blue early-type, or post-merger galaxy. We thus do not compute t_i for $\log(M/M_\odot) > 11.3$.

5.3. Comparing the Mass Functions of Major Mergers and Red Early-type Galaxies

We expect the red early-type stage to be the final phase in the evolution of major-merger-quenched galaxies. By comparing the shapes of the red early-type mass function and the major-merger mass function, we can make inferences about the

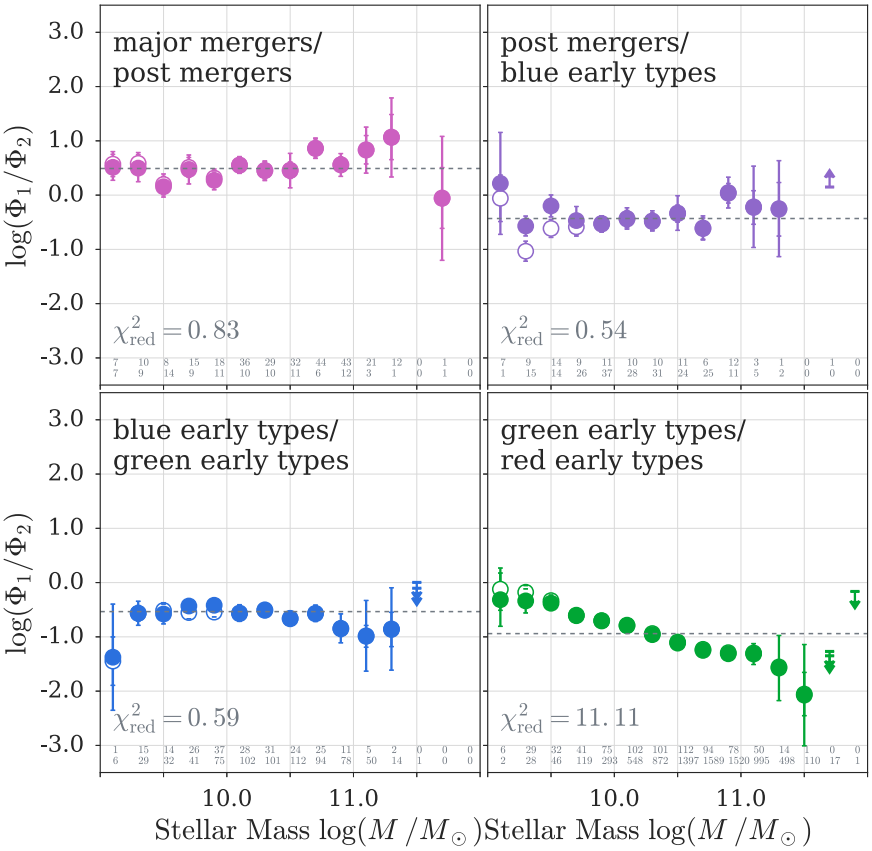

Figure 8. Transition curves for the major-merger sequence. We expect the stellar mass functions of galaxies evolving from the major-merger toward the red early-type stage to have similar shapes if none of the transitions are mass dependent. To test if this is the case and make a possible mass dependence more apparent, we take the ratio between the stellar mass functions of consecutive stages. We refer to these functions as "transition curves" and expect them to be flat if there is no mass dependence. From top left to bottom right, we show the transition curves for the major-merger to post-merger, post-merger to blue early-type, blue early-type to green early-type, and green early-type to red early-type stages. Open and filled symbols show the ratio based on the $1/V_{\rm max}$ and SWML results, respectively. To compute upper and lower limits, we also use the $1/V_{\rm max}$ and SWML Φ values, which is why in some panels we show two limits for the same mass bin. The horizontal dashed lines show the best-fitting relation if we assume a constant fraction. The corresponding $\chi^2_{\rm reduced}$ values are given within the panels. Note that upper and lower limits are not included in the fit. We also show the number of objects in each mass bin at the bottom of each panel. The upper and lower rows show the number of galaxies that were used to generate the numerator and denominator stellar mass functions, respectively. This figure illustrates that while the transition curves in the top three panels are consistent with being flat, there is a clear mass dependence between the green and red early-type stages (bottom right-hand panel). We explore this trend and its implications more in Section 5.3.

physical mechanisms that might be building up the red sequence.

We make the following statement:

1. if all red early-type galaxies have been quenched through major mergers,
2. and if red early-type galaxies do not gain significant amounts of mass while on the red sequence,

the mass function of red early-type galaxies should resemble the mass function of major mergers.

As discussed in Section 4.4, we expect galaxies evolving along the major-merger quenching sequence to not increase their stellar mass significantly, thereby maintaining the same mass distribution. On the red sequence, major-merger-quenched galaxies accumulate. This leads to an increase in their number density over time. The shape of their stellar mass function however stays constant, if they do not gain significant amounts of mass. The red early-type mass function should thus be as flat as the mass functions of the previous stages along the merger quenching sequence, if the aforementioned assumptions are true.

When discussing the transition curves in Section 5.1, we already pointed out that the green and red early-type mass functions have significantly different shapes. In Figure 10, we compare the major-merger mass function to the mass functions of red early-type galaxies.

The red early-type mass function has a significantly different shape compared to the major-merger mass function. While the major-merger mass function is fit with a flat single Schechter function, the red early-type mass functions has a strong double Schechter form.

This contradicts our expectations outlined above and implies that:

1. the mass function of red early-type galaxies has evolved with time,
2. or that the process of major-merger quenching and thus the major-merger mass function have evolved with time,
3. or that red early-type galaxies can be created through an alternative physical process, not just major-merger quenching.

The only way a red galaxy can increase its stellar mass significantly is through a dry merger. P10 discuss the effect that dry merging might have on the red stellar mass function shape.

They argue that dry mergers can primarily affect the steep high-mass end of the stellar mass function. To investigate the

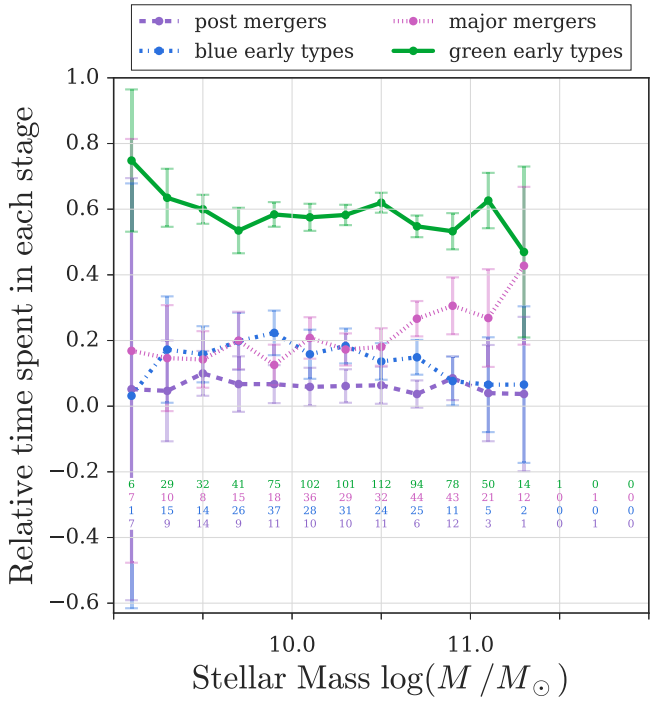

Figure 9. Fraction of time spent in stages along the major-merger sequence relative to the total time it takes to transition from the major-merger to the green early-type phase. We assume that the majority of galaxies transition from one stage to the next. Under this assumption, the number density of galaxies in a certain phase is proportional to the time spent in this phase. We use the stellar mass functions to compute the relative amount of time that galaxies spend in the major-merger, the post-merger, the blue early-type, and the green early-type stages. In the bottom part of the figure, we give the number of objects that we considered when computing the stellar mass functions and timescales. From top to bottom, we show the number of green early types, major mergers, blue early types, and post-mergers in each mass bin. Due to the low number density of high-mass galaxies, mass bins above $\log(M/M_{\odot}) = 11.3$ contain very few objects. Thus, we do not constrain the relative timescales for these bins.

change in the red mass function, they use a single Schechter function with $\alpha = -1.4$ and assume that 15% of all red galaxies undergo a 1:1 merger. Note that their dry merger probability is mass independent. After the merging, the new population of red galaxies consists of two groups: the 85% of red galaxies that did not undergo a major merger and retained their stellar mass function shape and the population of merged galaxies that has increased its M^* by 0.3 dex. Due to the major mergers, the new population of red galaxies contains fewer galaxies and has increased its stellar mass by 0.03 dex on average. When fitting the combined population of merged and unmerged galaxies with a single Schechter function, P10 find an M^* increase of 0.09 dex and a steepening of α by 0.15. The fact that M^* increased by 0.09 dex and not 0.03 dex is due to the degeneracy between α and M^* in the single Schechter fitting. Mergers with higher mass ratios will results in smaller changes in M^*. The simple model by P10 thus shows that dry mergers might lead to an increase in M^* and a steepening of α.

Based on the results by P10, we conclude that dry merging is unlikely to be the cause of the significant difference between the flat mass functions of the merging sequence and the red early-type mass function. For example, if the red early-type mass function had an initial shape similar to the green early-type mass function, dry merging would cause α_2 to decrease.

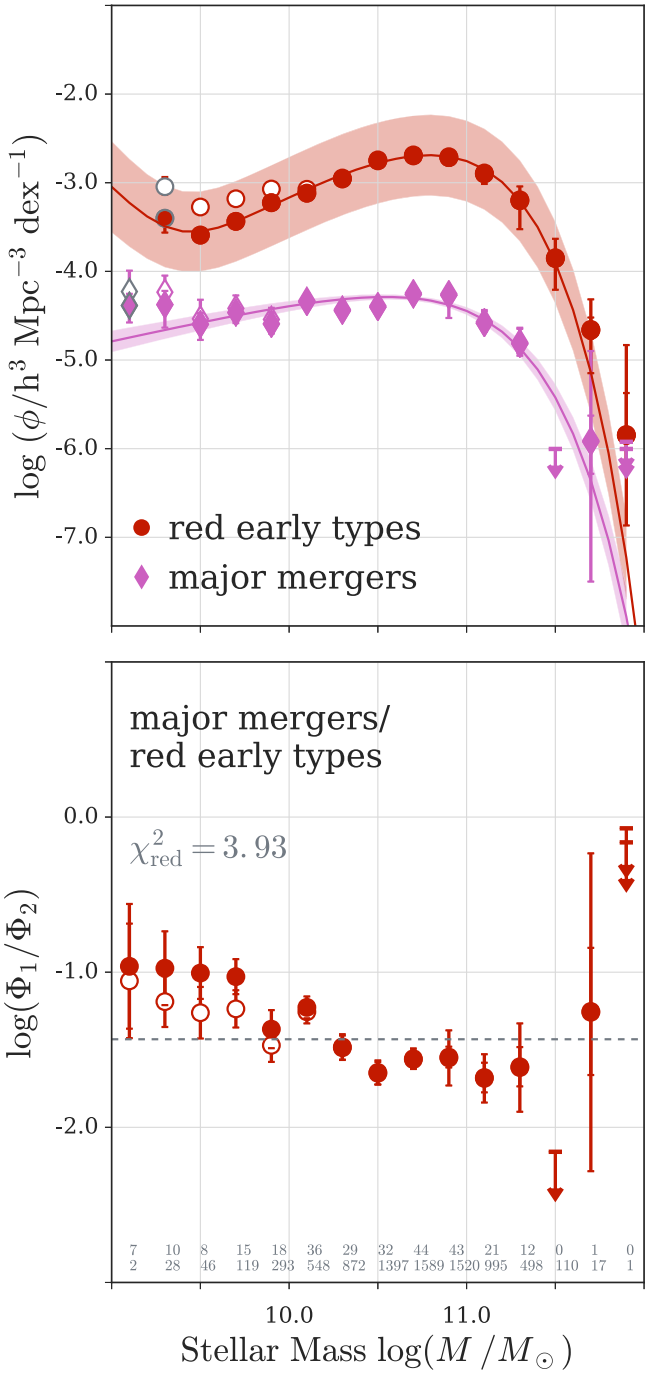

Figure 10. Stellar mass functions of major mergers and red early-type galaxies and the corresponding transition curve. The upper panel shows that major mergers and red early-type galaxies have significantly different stellar mass function shapes. This can also be seen in the bottom panel, which shows the transition curve for these two subsamples. As we discuss in the text, the significantly different shapes of the red early-type and the major-merger mass function imply that it is unlikely that all red early types have been quenched through the merger quenching process we observe in the local universe. Other quenching processes must either lead to the formation of red early-type galaxies, or the process of merger quenching and thus the major merger mass function must have evolved with time. In analogy to previous figures, we show the best-fitting constant fraction and the corresponding $\chi^2_{\rm reduced}$ value in the bottom panel. The number of objects in each mass bin is given at the bottom of the panel (numerator sample at the top, denominator sample at the bottom). In both panels, $1/V_{\rm max}$ and SWML results are shown with open and filled symbols, respectively. Upper limits are computed based on both methods.

Yet, we observe $\alpha_{2,\mathrm{red}} > \alpha_{2,\mathrm{green}}$. An evolution in the red early-type mass function due to dry merging that could explain the discrepancy between the major-merger and the red early-type mass functions which we observe at $z \sim 0$ is thus less likely.

A change in the major-merger mass function shape with time is possible. At higher redshift, major-merger quenching could for instance only lead to early-type formation at high stellar masses. Lower-mass galaxies could be gas rich enough to reform a disk and would thus not be part of the red early-type sample (De Lucia et al. 2011; Rodriguez-Gomez et al. 2016). This could lead to a build-up of red early-type galaxies at high stellar masses, thus explaining the strong double Schechter function shape that we observe at $z \sim 0$. Repeating the analysis at higher redshift would allow us to test this possibility. In the local universe, the reforming of a disk at low stellar masses is unlikely to be a significant effect. Low-mass galaxies that reform a disk would be part of the major merger, but, for instance, not the blue early-type sample. This would cause major mergers and galaxies in subsequent stages to have different mass function shapes, which is inconsistent with the observations (see Section 5.1).

The red early-type mass function shape could also be explained by the existence of alternative quenching channels. Major-merger quenching explains the existence of elliptical galaxies in the green valley. The green valley transition zone does however also include late types and indeterminates, which are galaxies that, based on their vote fraction distribution, canbe classified neither as clear early nor as clear late types (see Section 2.1). Late types and indeterminates are less likely to have been quenched through major mergers and could, through changes in their morphology, become part of the red early-type population.

The shape of the red early-type mass function therefore implies that it is unlikely that all red early-type galaxies have been created through the major-merger quenching process that we observe today. Alternative quenching channels must lead to red early-type formation or merger quenching at higher z must have led to a different mass function shape.

5.4. Comparing the Mass Functions of Major Mergers and Green Galaxies

In analogy to the previous section, we compare the stellar mass function shapes of major mergers and green galaxies. Figure 11 shows the stellar mass functions of major mergers and green galaxies in the top panel and the ratio of these functions in the bottom panel.

Based on our assumptions, we expect the mass function of green galaxies that are merger remnants to be similar in shape to the major-merger mass function. If the majority of green galaxies were merger quenched, the mass function of green galaxies should also resemble the major-merger mass function. The bottom panel of Figure 11 shows that the green and the major-merger mass functions have significantly different shapes. The green galaxy population does therefore not only consist of major-merger-quenched galaxies and must be dominated by a population of galaxies that have been quenched through alternative quenching channels.

Note that this argument is only based on the shapes of the major-merger and the green galaxy mass functions and the assumptions that merger-quenched galaxies reach the green valley at some point and do not gain significant amounts of mass during their evolution. This statement is independent of the mass functions of post-mergers, blue early types, and green early types, and therefore does not depend on morphological classifications.

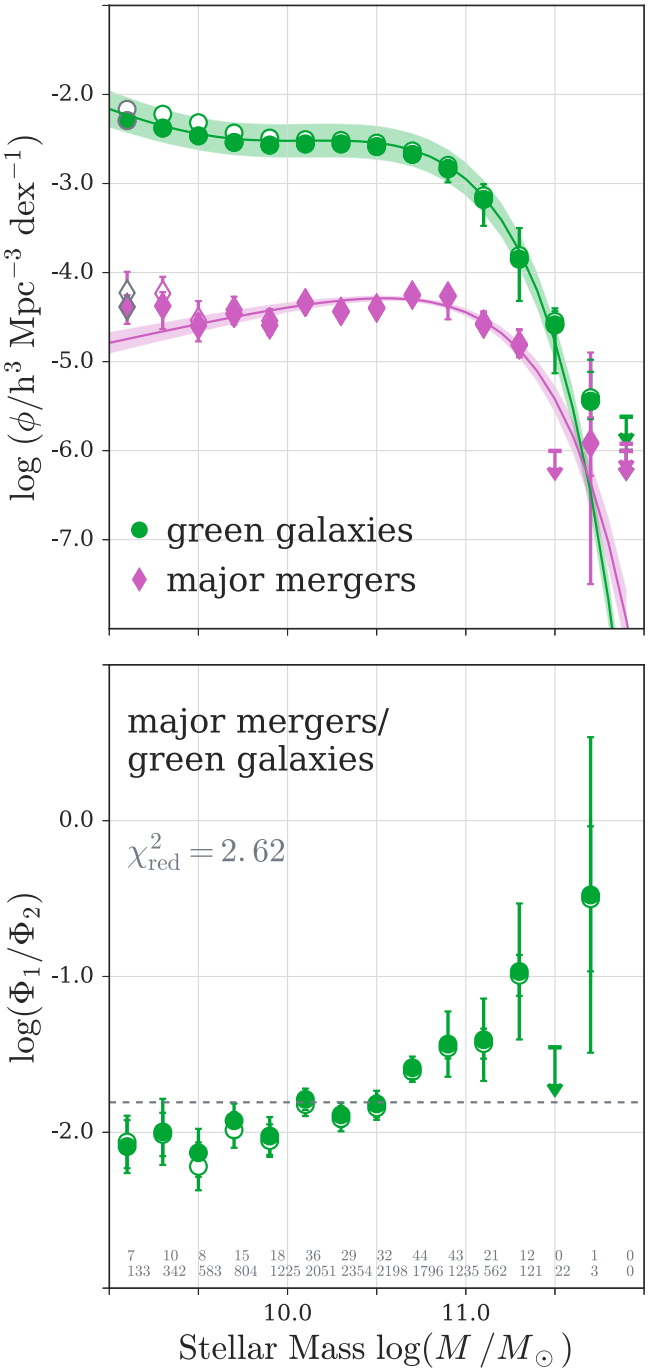

Figure 11. Stellar mass functions of major mergers and green galaxies, and the corresponding transition curve. The figure illustrates that major mergers and green galaxies have significantly different mass function shapes. This implies that not all green galaxies have been major-merger quenched and that the green valley is likely to be dominated by a population of galaxies that have been quenched through alternative quenching channels. This argument is only based on the mass functions presented here and does not depend on morphological classifications. For the mass function ratio, we indicate the best-fitting constant fraction with a dashed line and show the corresponding $\chi^2_{\mathrm{reduced}}$ value. The numbers in the bottom panel show the number of objects per mass bin (upper row: major mergers, bottom row: green galaxies). The $1/V_{\mathrm{max}}$ and SWML results are shown with open and filled symbols, respectively. Upper limits are computed based on both methods.

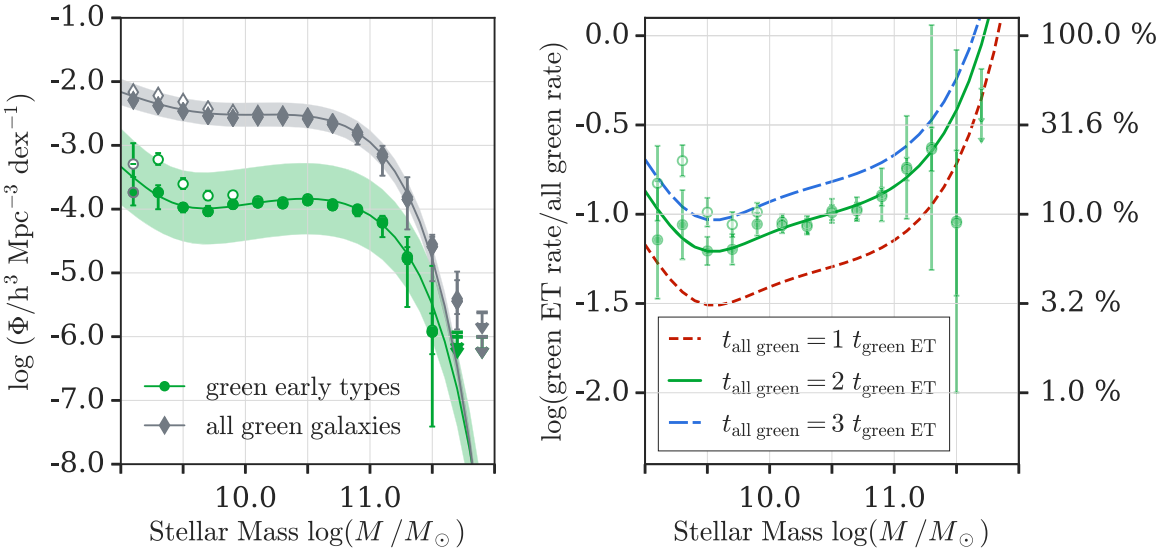

Figure 12. Major-merger contribution to quenching at $z \sim 0$. To estimate the contribution of major-merger quenching to the quenching of galaxies in the local universe, we use the number density of early types in the green valley. These galaxies are likely to have experienced a major merger in the past and will reach the red sequence in the future. In the left-hand panel, we show the stellar mass functions of all green and green early-type galaxies. The number density of green early types is significantly lower than the number density of all green galaxies. For instance, the difference in Φ^* is ∼1.3 dex, corresponding to ∼5%. From this we could already conclude that major-merger-quenched galaxies only make up a small fraction of all galaxies that are quenching at $z \sim 0$. However, Schawinski et al. (2014) and Smethurst et al. (2015) have shown that the green valley transition time is morphology dependent. Green early-type galaxies tend to transition the green valley on shorter timescales than late-type galaxies. This increases the merger quenching contribution to the green valley flux and quenching at $z \sim 0$. In the right-hand panel, we show the green early-type transition rate relative to the transition rate of all green galaxies. For the short dashed, solid, and long dashed lines, we assumed that on average green early types cross the green valley as fast as, two times as fast as, and three times as fast as all green galaxies. These ratios are based on the STY results. For clarity we show the ratio based on the $1/V_{\rm max}$ (open symbols) and SWML (filled symbols) results for $t_{\rm all\ green} = 2t_{\rm green\ ET}$ only. The precise value of the flux ratio depends on, for example, the definition of the green valley and the vote fraction threshold used for the morphological classifications. Nonetheless, this figure illustrates that major-merger-quenched galaxies are unlikely to make up the majority of galaxies transitioning the green valley at $z \sim 0$. Due to their low number density, this holds even if we take morphology-dependent green valley transition times into account.

5.5. Merger Contribution to the Flux through the Green Valley

After the very general arguments in the previous sections, we now use the green early-type mass function to discuss the significance of merger quenching at $z \sim 0$ in more detail. In Section 5.6, we model the redshift evolution of the red sequence and determine the fraction of galaxies that have been quenched through major mergers.

Galaxies that lie in the green valley at $z \sim 0$ are currently transitioning from the blue cloud to the red sequence. They have experienced a physical process that initiated their change in color in the past, and they will be reaching the red sequence in the future. In Section 4.2, we discussed why major-merger-quenched galaxies appear to already have an early-type morphology once they enter the green valley. In the following discussion, we will assume that the majority of green early-type galaxies have been quenched through major mergers. Morphologies then allow us to identify merger-quenched galaxies and to estimate their contribution to quenching at $z \sim 0$.

In the left-hand panel of Figure 12, we show the stellar mass functions of green early-type galaxies and of all green galaxies. The figure illustrates that green early-type galaxies only make up a small fraction of the green valley population. The difference in Φ^*, for instance, is ∼1.3 dex, corresponding to ∼5%.

Schawinski et al. (2014) use the NUV−optical color−color diagram to investigate the evolution of early- and late-type galaxies across the green valley. They show that early-type galaxies transition the green valley on a timescale on the order of 1 Gyr, whereas late-type galaxies evolve on a timescale on the order of several Gyr. Using a Bayesian approach, Smethurst et al. (2015) use τ-models to constrain the star formation history of individual galaxies. They measure a range of quenching timescales for smooth- and disk-like galaxies. In the green valley and at $z \lesssim 2$, the majority of bulge- and disk-dominated galaxies quench on intermediate ($1 < \tau/{\rm Gyr} < 2$) and slow ($\tau/{\rm Gyr} > 2$) timescales, respectively. Rapid quenching timescales ($\tau/{\rm Gyr} < 1$) are more likely to be found for smooth-like than disk-like galaxies.

Green early-type galaxies make up a small fraction of the total *number* of green galaxies. Yet their contribution to the overall number *flux* of galaxies across the green valley increases, if on average they evolve faster than the entire green valley population.

We use stellar mass functions to compare the number flux of green early-type galaxies to the number flux of all green galaxies. We weigh the stellar mass functions of green early types and of all green galaxies with the corresponding green valley transition times ($t_{\rm green\ ET}$, $t_{\rm all\ green}$) and determine the ratio of these rates. Note that the transition times we use here do not correspond to the τ-model quenching timescale, i.e., they do not describe the exponential decline of the SFR. Instead, $t_{\rm green\ ET}$ and $t_{\rm all\ green}$ correspond to the average green valley transition time of green early-type and all green galaxies. The contribution of green early types to the overall green valley flux is proportional to the ratio of $t_{\rm green\ ET}$ to $t_{\rm all\ green}$ and not their absolute values.

The right-hand panel of Figure 12 illustrates our results. We show the ratio of the green early-type rate to the overall green rate for $t_{\rm all\ green}/t_{\rm green\ ET} = 1, 2, 3$. For instance, using the result by Schawinski et al. (2007, 2014) and assuming $t_{\rm green\ ET} \sim 1$ Gyr, this implies that all green galaxies transition the green valley within $1 - 3$ Gyr. Note that a factor of three difference in the green valley transition times can correspond to an orders of

magnitude difference in terms of τ. The lines show the ratio based on the STY results. For clarity, we show the results based on $1/V_{\rm max}$ and SWML for $t_{\rm all\ green}/t_{\rm green\ ET} = 2$ only. The green galaxy sample contains few objects at high stellar masses. This is reflected by upper limits and large error bars at the high-mass end of the green and the green early-type mass functions. The high-mass end of the flux ratio is thus affected by large uncertainties. The upturn at $\log M \gtrsim 11$ in the right-hand panel of Figure 12 should hence not be taken at face value. Figure 12 shows that at a given stellar mass between $9 < \log(M/M_{\odot}) < 11$, green early-type galaxies make up ∼3%–30% of the the overall green valley flux if $1 < t_{\rm all\ green}/t_{\rm green\ ET} < 3$.

We stress that the fraction of ∼3%–30% represents a zeroth-order estimate. Besides being proportional to $t_{\rm all\ green}$ and $t_{\rm green\ ET}$, the fraction does, for instance, depend on the distribution of quenching times, i.e., the times at which galaxies start their evolution from the blue cloud to the red sequence. Furthermore, the definition of the green valley and the green early-type sample affects the results. As we have discussed in Section 2.1, the morphological classifications we use are based on the vote fractions of Galaxy Zoo users. For example, lowering the vote fraction cut above which we define a galaxy as an early type would result in some of the galaxies that are currently part of the indeterminate category to be assigned to the early-type sample. The number of green early-type galaxies and thus their contribution to the green valley flux would increase. We also assume that the majority of green early-type galaxies at $z \sim 0$ have been quenched through major mergers. If alternative quenching processes lead to the formation of green early-type galaxies, assuming that major-merger-quenched galaxies account for ∼ 3%–30% of the green valley flux would be an overestimate.

The analysis presented in this section does, however, show that it is unlikely that the majority of galaxies that are transitioning the green valley at $z \sim 0$ have been quenched through major mergers. This is due to the low number of green early-type galaxies and holds even if we take into account that the green valley transition time does depend on morphology.

5.6. Merger Contribution to the Build-up of the Red Sequence

To estimate how much quenching through major mergers could have contributed to the development of the red sequence, we model the evolution of the major-merger and the red galaxy mass functions over the redshift range $0 \leqslant z \leqslant 0.5$.

In addition to the points outlined in Section 4.1, we make the following assumptions.

1. Most galaxies that were involved in a major merger transition to the red sequence (see our discussion in Section 4.3).
2. It takes galaxies of the order of $t_{\rm mm} \sim 1$ Gyr to transition from the major-merger to the red early-type stage (see e.g., Springel et al. 2005a).
3. The major-merger mass function retains its $z \sim 0$ shape and does not change with z.
4. The normalization of the major-merger mass function increases as $(1 + z_{\rm mm})^{\beta}$. Based on Bridge et al. (2010), we use $\beta = 2.25$.

So far, previous studies have primarily studied the redshift evolution of the integrated merger fraction (see, e.g., Bridge et al. 2010; Lotz et al. 2011; Keenan et al. 2014; Robotham et al. 2014). Studying how the merger-mass function, or equivalently, the merger fraction as a function of stellar mass, evolves with z is more challenging. We assume that the merger mass function retains its shape and that only Φ^* increases with increasing z. This represents the simplest and most straightforward assumption that we can make until the z evolution of the merger-mass function has been constrained observationally.

First, we motivate our assumption for $t_{\rm mm}$. Second, we estimate the number density of major-merger-quenched galaxies reaching the red sequence within a z interval. Third, we find an analytic expression for the number density of newly quenched galaxies within a redshift interval. By comparing the two quantities and integrating over z, we determine the contribution of major-merger-quenched galaxies to the build-up of the red sequence.

5.6.1. Timescales

Observationally, it is challenging to determine the average time that it takes a galaxy to evolve from the major-merger to the red early-type stage. Besides visual classification, common methods to identify major mergers include the close pair technique (see e.g., Patton et al. 2000; Ellison et al. 2008) and morphological measurements based on CAS (see, e.g., Conselice 2003), the Gini coefficient, or M_{20} (see e.g., Lotz et al. 2004). Although these techniques allow the measurement of the merger fraction, estimating the merger rate is less straightforward and can lead to disagreement among the methods (Lotz et al. 2011). For the CAS method, Bertone & Conselice (2009) use a sensitivity timescale of 0.4 to 1 Gyr, and for the close pair technique, Patton et al. (1997) assume an infall time of the order of a few hundred million years.

Using simulations, both Springel et al. (2005a) and Hopkins et al. (2008b) find that merging galaxies significantly change their optical color and decrease their SFR within less than 1 Gyr if AGN feedback is considered. Also invoking AGN feedback, Kaviraj et al. (2011) use a phenomenological model to reproduce the ∼1 Gyr-long blue to-red evolution of elliptical galaxies, which was previously observed by Schawinski et al. (2007).

For our simple model, we thus assume $t_{\rm mm} \sim 1$ Gyr for the average transition time between the major-merger and the red early-type stage. In Figure 17, we furthermore show that the chosen $t_{\rm mm}$ value does not significantly affect our results by varying $t_{\rm mm}$ from 0.5 to 3 Gyr.

5.6.2. The Evolution of the Major-merger Mass Function

In the top middle panel of Figure 3, we show the ratio between the major-merger mass function and the mass function of all blue galaxies. We can interpret this ratio as the merger fraction relative to all blue galaxies and rewrite the major-merger mass function as

$$\Phi_{\rm mergers}(z = 0, M) = {\rm frac}(M)\Phi_{\rm blue}(z = 0, M). \quad (7)$$

We determine the mass function of galaxies that were quenched through a major merger and are reaching the red sequence at redshift z by considering the blue galaxy mass function at the merging time, $z_{\rm mm}$ ($z_{\rm mm} - z \triangleq t_{\rm mm} \sim 1$ Gyr). The mass function of galaxies that are reaching the red sequence at z and were involved in a major merger at $z_{\rm mm}$ can thus be

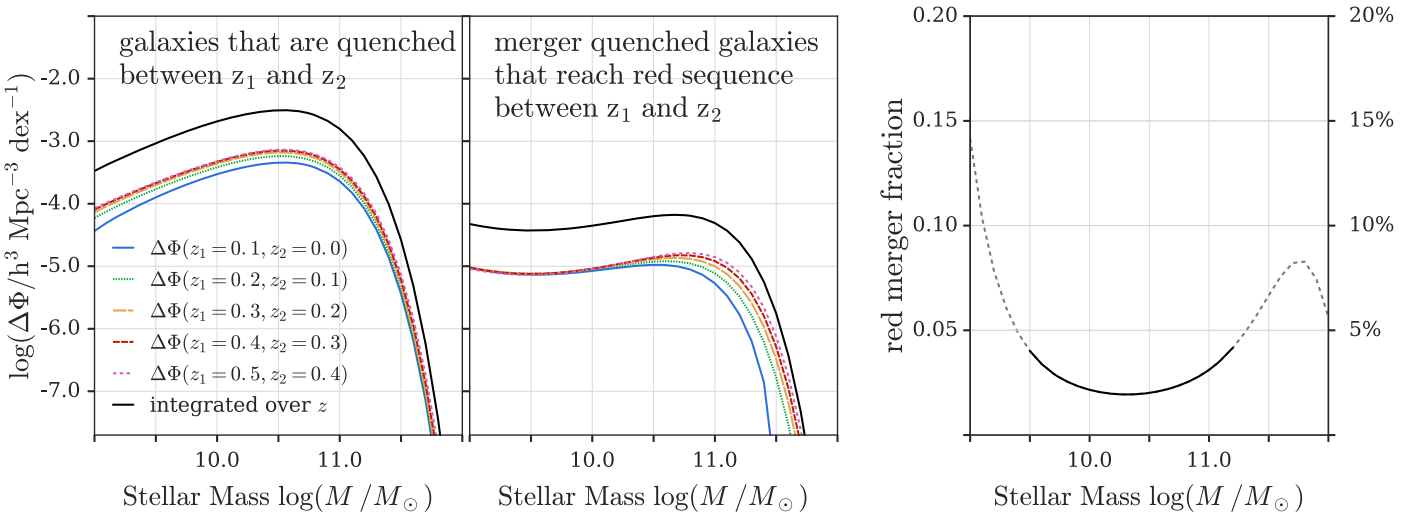

Figure 13. Contribution of merger-quenched galaxies to the build-up of the red sequence between $0 \leqslant z \leqslant 0.5$. We model the evolution of the red (left-hand panel) and the major-merger mass function (middle panel) to determine what fraction of red galaxies was quenched through major mergers (right panel). To estimate the number density of mass-quenched galaxies between z_1 and z_2 ($z_1 > z_2$), we predict the shape of the blue mass function at z_2 by evolving the blue galaxies along the main sequence and then subtracting the true, blue mass function at z_2. We model the redshift evolution of the major-merger mass function by combining our measurement of the merger fraction at $z \sim 0$ (see Figure 3) with the redshift evolution of the blue mass function (Caplar et al. 2015) and a redshift-dependent normalization to allow for more merging at higher z (Bridge et al. 2010). We then derive the mass function of merger-quenched galaxies by assuming that it takes a galaxy about 1 Gyr to transition from the major-merger to the red early-type stage. We integrate over z and measure the contribution of merger quenching to the red sequence by taking the ratio of all merger-quenched and all mass-quenched galaxies. We show the red merger fraction as a function of stellar mass in the right-hand panel. The dashed line shows the masses where the major-merger (low-mass and high-mass end) and the red stellar mass functions (high-mass end) are affected by significant uncertainties.

expressed as

$$\Phi_{\text{red mergers}}(z, M) = (1 + z_{\text{mm}})^{\beta} \text{frac}(M) \Phi_{\text{blue}}(z_{\text{mm}}, M). \quad (8)$$

Equation (8) shows that we need to model the redshift dependence of the blue stellar mass function to be able to estimate the major-merger contribution to the red sequence. We use the results of Caplar et al. (2015), who derive an analytic expression for the change in Φ^*_{blue} and M^*_{blue} using data from Ilbert et al. (2013). The redshift evolution of the blue mass function can then be expressed as

$$\begin{aligned} \Phi_{\text{blue}}(M, z) d\log M &= \ln(10) \Phi^*_{\text{blue}}(z) e^{-(M/M^*_{\text{blue}}(z))} \\ &\quad \times \left(\frac{M}{M^*_{\text{blue}}(z)}\right)^{\alpha_{\text{blue}}+1} d\log M \\ \log \Phi^*_{\text{blue}}(z) &= a_0 + a_1\kappa + a_2\kappa^2 + a_3\kappa^3 \\ \log M^*_{\text{blue}}(z) &= b_0 + b_1\kappa + b_2\kappa^2 + b_3\kappa^3, \end{aligned} \quad (9)$$

with $\kappa = \log(1 + z)$. We adopt the following parameter values from Caplar et al. (2015): $a_1 = -0.26$, $a_2 = -1.6$, $a_3 = -0.88$ and $b_1 = -0.53$, $b_2 = 3.36$, $b_3 = -3.75$. We adjust α_{blue}, a_0 and b_0 so that at $z = 0$, Φ_{blue} corresponds to the best-fit Schechter function of blue galaxies that we determined in Weigel et al. (2016). We thus assume $\alpha_{\text{blue}} = -1.21$, $a_0 = -2.43$ and $b_0 = 10.6$.

By combining Equations (8) and (9), we can model the evolution of $\Phi_{\text{red mergers}}(z, M)$, the stellar mass function of galaxies that have been quenched through major mergers at z_{mm} and are reaching the red sequence at z. The number density of merger-quenched galaxies that reach the red sequence between z_1 and z_2 ($z_1 > z_2$) is given by

$$\begin{aligned} \Delta\Phi_{\text{red mergers}}(z_1, z_2, M) &= \Phi_{\text{red mergers}}(z_1, M) \\ &\quad - \Phi_{\text{red mergers}}(z_2, M). \end{aligned} \quad (10)$$

The central panel of Figure 13 shows $\Delta\Phi_{\text{red mergers}}$ for a range of z_1 and z_2 values.

5.6.3. The Evolution of the Red Mass Function

To estimate the contribution of major-merger-quenched galaxies to the red sequence within the last ~5 Gyr, we also need to model the evolution of the mass function of red galaxies.

To determine the number density of galaxies that reach the red sequence between z_1 and z_2, we evolve the blue galaxies along the main sequence. Using Equation (9), we generate the mass function of blue galaxies at $z = z_1$. Without quenching, these galaxies will continue to evolve along the main sequence and will gain mass. We use the main sequence equation by Lilly et al. (2013) to estimate this change in stellar mass between z_1 and z_2, and predict the shape of the blue mass function at $z = z_2$. We measure the mass function of newly quenched objects between z_1 and z_2 by subtracting the true blue mass function at $z = z_2$ from our prediction. We express the number density of newly quenched objects between z_1 and z_2 in the following way:

$$\begin{aligned} M^*(z_2) &= M^*_{\text{blue}}(z_1) \cdot (1 + sSFR(z_1) \cdot t) \\ \Phi_{\text{predicted blue}}(z_2, M) &= \ln(10) \Phi^*_{\text{blue}}(z_1) \\ &\quad \times e^{-M/M^*(z_2)} \left(\frac{M}{M^*(z_2)}\right)^{\alpha_{\text{blue}}(z_1)+1} \\ \Delta\Phi_{\text{new red}}(z_1, z_2, M) &= \Phi_{\text{predicted blue}}(z_2) - \Phi_{\text{true blue}}(z_2). \end{aligned} \quad (11)$$

Here, t corresponds to the time between z_1 and z_2 in Gyr. For the predicted blue mass function, we keep Φ^* and α constant and simply shift M^* toward higher stellar masses. We show the number density of newly quenched galaxies in the red sequence in the left panel of Figure 13.

5.6.4. Comparing Merger-quenched Galaxies to All Quenched Galaxies

With Equations (8) and (11), we estimate the contribution of major-merger-quenched galaxies to the red sequence between $0 \leqslant z \leqslant 0.5$. We bin in redshift space and estimate the number density of all quenched and of merger-quenched galaxies by computing

$$\Phi_{\sum \text{new red}}(M) = \sum_{i}^{N_{z-\text{bins}}} \Delta\Phi_{\text{red}}(z_i,\, z_i - \Delta z,\, M),$$
$$\Phi_{\sum \text{red mergers}}(M) = \sum_{i}^{N_{z-\text{bins}}} \Delta\Phi_{\text{red mergers}}(z_i,\, z_i - \Delta z,\, M). \quad (12)$$

The major-merger contribution to the build-up of red sequence is then given by

$$\text{red merger fraction}(M) = \frac{\Phi_{\sum \text{red mergers}}(M)}{\Phi_{\sum \text{new red}}(M)}. \quad (13)$$

We show the red merger fraction as a function of stellar mass in the right-hand panel of Figure 13. When interpreting the results, it is important to be aware that at the high-mass end, both the red and the major-merger $z \sim 0$ mass functions are affected by significant uncertainties. For the major-merger mass function, this is also the case at the low-mass end (see Figure 10). These uncertainties also affect the red merger fraction shown in Figure 13. At these masses, we thus show the red merger fraction with a dashed line.

As a reference, we show the evolution of the blue mass function and the mass function of merger-quenched galaxies reaching the red sequence in Figure 16. With decreasing redshift, the number density of blue galaxies increases. Yet even though $\Phi_{\text{red mergers}}$ depends on Φ_{blue}, the number density of red merger-quenched galaxies decreases with decreasing redshift. This is due to the $(1+z)^{\beta}$ factor, which we have introduced in Equation (8). $(1+z)^{\beta}$ decreases more steeply than Φ^{*}_{blue} increases. This causes fewer merger-quenched galaxies reaching the red sequence at lower redshift.

Once we have determined $\Phi_{\sum \text{new red}}(M)$, we can also estimate the fraction of red galaxies that has been quenched within the last 5 Gyr. We integrate $\Phi_{\sum \text{new red}}(M)$ and the mass function of all red galaxies (see Table 1) between $10^9\,M_{\odot}$ and $10^{12}\,M_{\odot}$. Over this mass range, galaxies that have been quenched within $0 \leqslant z \leqslant 0.5$ make up about 41% of all red galaxies.

We conclude that based on the approach presented here, the contribution of major-merger-quenched galaxies to the build-up of the red sequence within the last 5 Gyr is 1%–5% at a given mass. Within this time range, a significant fraction of galaxies has been quenched; the contribution of merger-quenched galaxies is, however, negligible. This is in agreement with our results for the local universe where we found the number flux of green early-type galaxies across the green valley to be low compared to the total green valley flux (see Section 5.5).

5.7. The Significance of Major-merger Quenching

We discussed the significance of major-merger quenching in Sections 5.3–5.6. Our first test consisted of comparing the major-merger to the red early-type mass function. Their different shapes let us to conclude that it is unlikely that all red early-type galaxies have been created through the major-merger quenching process that we observe today. Our second analysis was purely based on the stellar mass functions of green galaxies and of major mergers. By comparing their shapes, we concluded that the local green valley population is dominated by galaxies that are unlikely to have been quenched through major mergers. This straightforward argument is independent of the mass functions of later stages along the merger sequence and independent of the early-type morphological classifications. For our third analysis, we used the stellar mass functions of green early types and of green galaxies. We argued that green early types, which are likely to have been merger quenched, only make up a small fraction of all green galaxies. Even if we take into account that early types tend to transition the green valley on timescales shorter than the total green population, merger-quenched galaxies are unlikely to make up the majority of the overall green valley flux at $z \sim 0$. For our fourth approach, we modeled the evolution of the major-merger and the red mass function from $z = 0.5$ to $z = 0$. We concluded that merger-quenched galaxies account for 1%–5% of all galaxies that quenched within the last 5 Gyr.

All four tests are independent from each other, yet their results are consistent: merger quenching is unlikely to contribute significantly to the quenching of galaxies at $z \sim 0$ and is unlikely to have quenched the majority of galaxies that reached the red sequence within the last 5 Gyr. To explain the existence of the green valley and the red sequence populations, at least one additional quenching mechanism has to exist. To account for the slow transition rate of green valley galaxies, alternative quenching channels are likely to lead to a change in color that is slow compared to major-merger quenching. As we have discussed in Section 5.3, alternative quenching processes could also lead to the formation of red early-type galaxies, thereby explaining the shape of the red early-type mass function.

6. Discussion

6.1. The Role of AGNs in the Quenching of Star Formation

In Section 5, we argued that major-merger quenching alone is unlikely to account for the quenching of all galaxies that we observe in the local universe. Lofthouse et al. (2017) come to a similar conclusion for major merger quenching at $z \sim 2$. Alternative quenching channels have to be introduced to explain the properties of the total green valley and red sequence population. For example, the slow evolution of green late types is likely to be caused by a quenching process that does not involve major mergers. As we discussed in Section 3.3, quenching could also be caused by secular processes (Kormendy & Kennicutt 2004; Masters et al. 2011; Cheung et al. 2013), environmental processes such as ram pressure stripping (Gunn & Gott 1972) or strangulation (Larson et al. 1980; Balogh et al. 2000), or AGN feedback (Silk & Rees 1998; Di Matteo et al. 2005; Schawinski et al. 2006; Kauffmann et al. 2007; Georgakakis et al. 2008; Cattaneo et al. 2009; Hickox et al. 2009; Fabian 2012; Bongiorno et al. 2016; Smethurst et al. 2016).

On one side, AGN feedback seems to be necessary to efficiently transform major-merger remnants from blue to red early types. For instance, Springel et al. (2005a) show that after a gas-rich merger, AGN feedback is necessary to move the merger remnant from the blue cloud to the red sequence. Without AGN feedback, low levels of star formation ensure that the galaxy remains blue (also see, e.g., Birnboim et al.

2007; Hopkins et al. 2008b; Khalatyan et al. 2008). Similarly, Sparre & Springel (2016) also use hydrodynamical simulations to show that without strong AGN feedback, the newly formed galaxy can return to be a star-forming late type. Using a phenomenological model, Kaviraj et al. (2011) argue that if only star formation feedback is considered, the gas depletion rate is too low to explain the rapid transition of early-type galaxies from blue to red (Schawinski et al. 2006, 2014). AGNs are thus often found in morphologically disturbed galaxies or ULIRGs (e.g., Bennert et al. 2008; Urrutia et al. 2008; Yuan et al. 2010; Koss et al. 2011; Hong et al. 2015).

On the other hand, a major merger does not seem to be necessary for a black hole to be actively accreting (Ellison et al. 2011). For example, Treister et al. (2012) argue that only the most luminous AGNs are triggered through major galaxy mergers. Simmons et al. (2013) find AGNs in massive galaxies without classical bulges. These galaxies are unlikely to have experienced significant mergers in the past, which suggests that secular processes might be feeding the central black hole (see, e.g., Jogee 2006; Alexander & Hickox 2012).

AGN feedback could thus be involved in two separate quenching channels. First, in major mergers, AGN feedback might be a necessary, but not sufficient, condition for quenching. Second, if efficient enough, AGN feedback might be sufficient for the quenching of non-merger galaxies.

6.2. Close Pairs

D10 argue that their major-merger catalog probes the post-close-pair stage. Introducing a volume limit, they compare a catalog of SDSS close pairs (projected separation <30 kpc, line-of-sight velocity difference <500 km s^{-1}) to their sample of visually classified mergers. After eliminating pairs that are well separated and show no signs of interaction, $\sim$64% of all perturbed, remaining pairs have $f_{\rm m} < 0.4$ and are thus not part of the D10 sample. Yet D10 also claim a strong correlation between the merger vote fraction and the projected separation of two merging galaxies: the farther apart two galaxies are, the less likely they are to be classified as a merger. They thus argue that their selection technique is sensitive to merging systems that show clearer signs of interaction than typical close pair galaxies, therefore probing merging systems that have progressed from the close pair stage.

To compare our results to observations of galaxies in a stage that is likely to proceed to the D10 major-merger stage, we use the close pair study by Domingue et al. (2009). Using SDSS (DR5; Adelman-McCarthy et al. 2007) and Two Micron All Sky Survey (2MASS, Extended Source Catalog; Jarrett et al. 2000) data, Domingue et al. (2009) determine the luminosity function of close pairs. For all pairs, isolated pairs, and grouped pairs, they find slope α values of -1.03 ± 0.09, -0.8 ± 0.1 and -1.2 ± 0.2, respectively.

With $\alpha = -0.55 \pm 0.08$, we find an increasing slope for major mergers, whereas the luminosity function of all close pairs is almost flat. Our stellar mass function best-fitting parameters are based on the STY results. A shallower mass function for major mergers is thus less likely, yet not completely ruled out (see Figure 6). The slope of the isolated pair luminosity function is consistent with the slope of the stellar mass functions of our post-mergers, blue early types, and mergers in underdense regions (see Table 1). The slope of the grouped pair luminosity function is steeper and consistent with the slope of the blue galaxies' stellar mass function ($\alpha = -1.21 \pm 0.01$).

While our results are not directly comparable to the work by Domingue et al. (2009), it is interesting to note that the stellar mass and luminosity functions of close pairs and galaxies along the merger sequence are unusually flat. If close pairs and major mergers were randomly drawn from the entire or the blue galaxy population, we would expect their luminosity and mass function to have comparable, steeper slopes. This difference in slopes is also reflected in the mass-dependent merger fractions (see Figure 3). As we discussed in Section 3.2, the unusually shallow mass functions of close pairs and subsequent stages could be caused by a mass-independent dark matter halo merger fraction in combination with a mass-dependent stellar-to-halo mass conversion (Bertone & Conselice 2009; Hopkins et al. 2010a, 2010b; Behroozi et al. 2013).

6.3. Slow and Fast Rotators

We used the color of galaxies in combination with their morphological classifications to study the process of merger quenching. Morphological classifications were essential for our approach as these allowed us to follow galaxies that are likely to have been merger quenched along their evolution from the blue cloud to the red sequence. However, we have not yet included kinematic information in our approach. After projects such as SAURON (de Zeeuw et al. 2002), CALIFA (Sánchez et al. 2012), and ATLAS^{3D} (Cappellari et al. 2011), the next generation of IFU surveys, for example, the SAMI galaxy survey (Croom et al. 2012; Bryant et al. 2015), MaNGA (Bundy et al. 2015), and the Hector survey (Bland-Hawthorn 2015), will increase the number of observed galaxies by orders of magnitude. These surveys will allow us to move from studying single objects to including kinematic information in a statistical approach. In the context of quenching, the formation and evolution of slow and fast rotating galaxies (Illingworth 1977; Davies et al. 1983 and e.g., Cappellari 2016 and references therein) will be especially important. The formation of fast and slow rotators has been studied observationally (e.g., Forbes et al. 2016; Oh et al. 2016) and with numerical (e.g., Bois et al. 2010, 2011), semi-analytic (e.g., Khochfar et al. 2011), and hydrodynamical simulations (e.g., Naab et al. 2014). Although there seems to be a clear link between major mergers and slow and fast rotators, no simple model regarding their formation has emerged so far. Among other parameters, the amount of involved gas, the number of mergers in the past, the mass ratio, the amount and orientation of angular momentum of the merging galaxies, and the resulting spin up or spin down of the remnant seem to play a significant role in their evolution. Nonetheless, similar to morphologies, considering kinematics in the analysis of quenching will be very insightful. We will thus be exploring the role of slow and fast rotators in the context of merger quenching in future work.

7. Summary

We used SDSS DR7 and Galaxy Zoo 1 data in combination with visually selected major-merger and post-merger samples to determine the stellar mass functions of major mergers and post-mergers in the local universe (see Figure 2). These mass functions allowed us to constrain the fraction of major mergers and post-mergers relative to the entire galaxy sample and to blue and to red galaxies (see Figure 3). In Section 3.3, we

compared our measurement of the major-merger mass function to the empirical quenching model by P10. We concluded that the major-merger mass function in the local universe is inconsistent with the mass-independent, but environment-dependent merger quenching process that P10 proposed.

To investigate the process of major merger quenching and its significance in the local universe, we made three key assumptions (see Section 4):

1. merger-quenched galaxies pass through five distinct stages: major merger, post merger, blue early type, green early type, and red early type,
2. the probability of a galaxy evolving from the major-merger to the red early-type stage is mass independent and effects such as disk reforming, AGN feedback, dynamical friction, and the fading of merger features do not introduce a mass dependent bias,
3. while transitioning from the major-merger to the red early-type stage, galaxies do not gain significant amounts of stellar mass.

These three assumptions led us to the expectation that the stellar mass functions of galaxies in these five stages should be similar in shape if they represent an evolutionary sequence.

In addition to the major-merger and post-merger samples, we also determined the mass functions for galaxies in the blue, green, and red early-type stages. Using the ratio of mass functions of subsequent stages, we showed that galaxies in the major-merger, post-merger, and blue and green early-type stages indeed have similar mass function shapes (see Figure 8). We concluded that that major mergers are likely to lead to the quenching of star formation, with the five stages that we considered representing an evolutionary sequence from star formation to quiescence. The flat transition curves furthermore provide support for our assumption that the probability of merger remnants reaching the red early-type stage is likely to be mass independent.

The mass functions of galaxies along the sequence allowed us to constrain the relative amount of time spent in the major-merger, post-merger, blue early-type, and green early-type stages (see Figure 9). We assumed that the majority of galaxies transition from one stage to the next. Based on this assumption, we found that galaxies spend ∼60% of their time in the green early-type stage and ∼5% of their time in the post-merger stage.

To investigate the significance of major-merger quenching in the local universe, we used four tests that vary in their level of sophistication and assumptions.

1. We compared the shapes of the major-merger and the red early-type mass functions (see Figure 10) and concluded that it is unlikely that all red early types were created through the major-merger quenching process that we observe today. Alternative quenching channels are necessary to explain the red early-type mass function shape.
2. By comparing the major-merger and the green mass function shapes (see Figure 11), we argued that the green valley population is dominated by galaxies that are unlikely to have been major-merger quenched in the past.
3. We estimated the contribution of major-merger-quenched galaxies to the overall green valley number flux (see Figure 12). We concluded that green early-type galaxies, which are likely to have been major-merger quenched, are unlikely to dominate the $z \sim 0$ flux of galaxies across the green valley.
4. For our final test, we simulated the evolution of the red stellar mass function. We estimated the fraction of galaxies that are likely to have been merger quenched within the last 5 Gyr (see Figure 13) to be 1%–5% at a given stellar mass.

In summary, our analysis shows that major mergers are likely to lead to an evolution from star formation to quiescent via quenching. Yet merger quenching is unlikely to account for the majority of quenching, neither at $z \sim 0$ nor within the last 5 Gyr. To explain the existence of the green valley and red sequence population, alternative quenching channels, which are likely to lead to a slow green valley transition, have to exist.

We thank the anonymous referee for helpful comments. A.K.W. and K.S. gratefully acknowledge support from Swiss National Science Foundation Grants PP00P2_138979 and PP00P2_166159. B.D.S. acknowledges support from the National Aeronautics and Space Administration (NASA) through Einstein Postdoctoral Fellowship Award Number PF5-160143 issued by the *Chandra* X-ray Observatory Center, which is operated by the Smithsonian Astrophysical Observatory for and on behalf of NASA under contract NAS8-03060. This research made use of NASA's ADS Service. This publication made use of Astropy, a community-developed core PYTHON package for Astronomy (Astropy Collaboration et al. 2013) and the PYTHON plotting package matplotlib (Hunter 2007). This publication made extensive use of the Tool for OPerations on Catalogs And Tables (TOPCAT), which can be found at http://www.starlink.ac.uk/topcat/. The development of Galaxy Zoo was supported by the Alfred P. Sloan Foundation and The Leverhulme Trust. Funding for the SDSS has been provided by the Alfred P. Sloan Foundation, the Participating Institutions, the National Aeronautics and Space Administration, the National Science Foundation, the US Department of Energy, the Japanese Monbukagakusho, and the Max Planck Society. The SDSS Web site is http://www.sdss.org/. The SDSS is managed by the Astrophysical Research Consortium (ARC) for the Participating Institutions. The Participating Institutions are The University of Chicago, Fermilab, the Institute for Advanced Study, the Japan Participation Group, The Johns Hopkins University, Los Alamos National Laboratory, the Max-Planck-Institute for Astronomy (MPIA), the Max-Planck-Institute for Astrophysics (MPA), New Mexico State University, University of Pittsburgh, Princeton University, the United States Naval Observatory, and the University of Washington.

Appendix
Extended Analysis

A.1. The Effect of Stellar Mass Estimates on the Shape of the Major-merger Mass Function

As we discussed in Section 2.3, spectra for both merging galaxies are only available for 23% of all merging systems in the D10 catalog. D10 thus fit two-component star formation histories to the photometry to estimate the stellar masses of all merging galaxies. We use these stellar mass estimates to select major mergers. However, for the construction of the

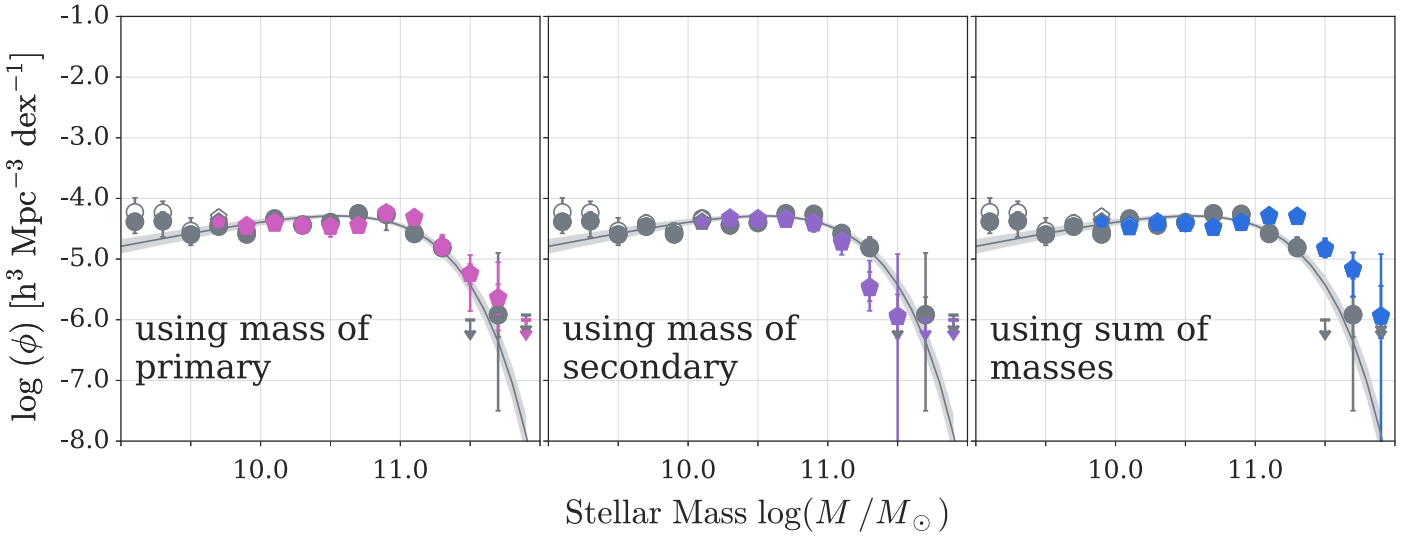

Figure 14. Effect of using the masses of the primaries, the secondaries, and the sum of the masses of the merging galaxies for the major mass function construction. To determine the major-merger mass function, which we use for our analysis and which we show in gray here, we use mass estimates from the MPA JHU catalog (Kauffmann et al. 2003; Brinchmann et al. 2004; Salim et al. 2007). As spectra are only available for some of the galaxies in the D10 catalog, this results in us using a mix of primary and secondary masses for the mass function determination. We use the photometry-based stellar mass estimates by D10 to show that this combination of mass estimates does not significantly affect the major-merger mass function shape. In the left-hand panel, we show the major-merger mass function based on the mass of the more massive merging partner. For the stellar mass function in the central panel, we used the mass of the secondaries as input. In the right-hand panel, we show the stellar mass function based on the sum of masses.

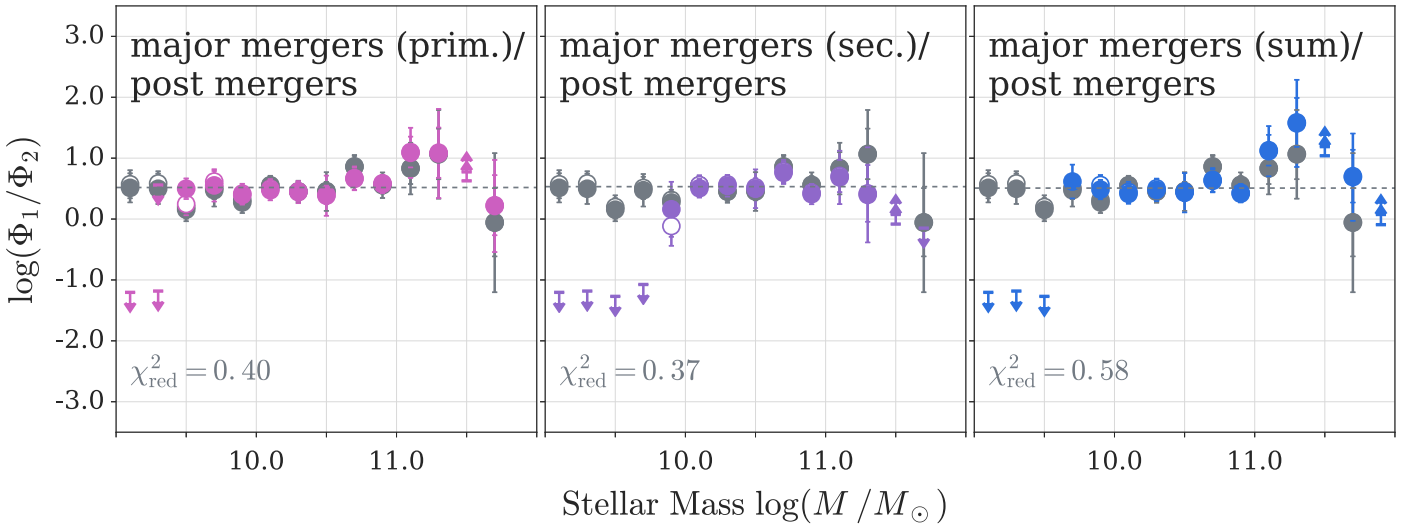

Figure 15. Ratio between the modified major-merger mass functions and the post-merger mass function. We use the major-merger mass functions shown in Figure 14 to construct the transition curves (see Section 5.1) relative to the post-merger sample. From left to right and in analogy to Figure 14, we use the mass function based on primary masses, secondary masses, and the sum of masses for the ratio. The horizontal dashed line shows the best-fitting relation if we assume a constant ratio between these modified merger mass functions and the post-merger mass function. The corresponding $\chi^2_{\rm red}$ values are given within the panels. Shown in gray is the ratio between the major-merger mass function, which we use for our analysis, and the post-merger mass function. Even though using the sum of stellar masses as input for the merger mass function leads to a shift in M^* (see the right-hand panel of Figure 14), the transition curve for mergers and post-mergers shows no significant mass dependence, as the right-hand panel shows.

major-merger mass function, which is for instance shown in Figure 6, we use stellar mass estimates from the MPA JHU catalog (Kauffmann et al. 2003; Brinchmann et al. 2004; Salim et al. 2007) to ensure consistency with the other mass functions used for our analysis. If both galaxies that are involved in a major merger have been observed spectroscopically, we use the mass of the more massive galaxy, the primary for the mass function construction. If a spectrum is only available for one of the two merging galaxies, we use the mass of the galaxy for which a spectrum is available. According to the D10 mass measurements, in 69% of all cases, the galaxy with the available spectrum corresponds to the primary. We now illustrate the effect of this approach on the shape of the major-merger mass function.

In Figure 14, we show three versions of the major-merger mass function. Each is based on a different set of stellar mass

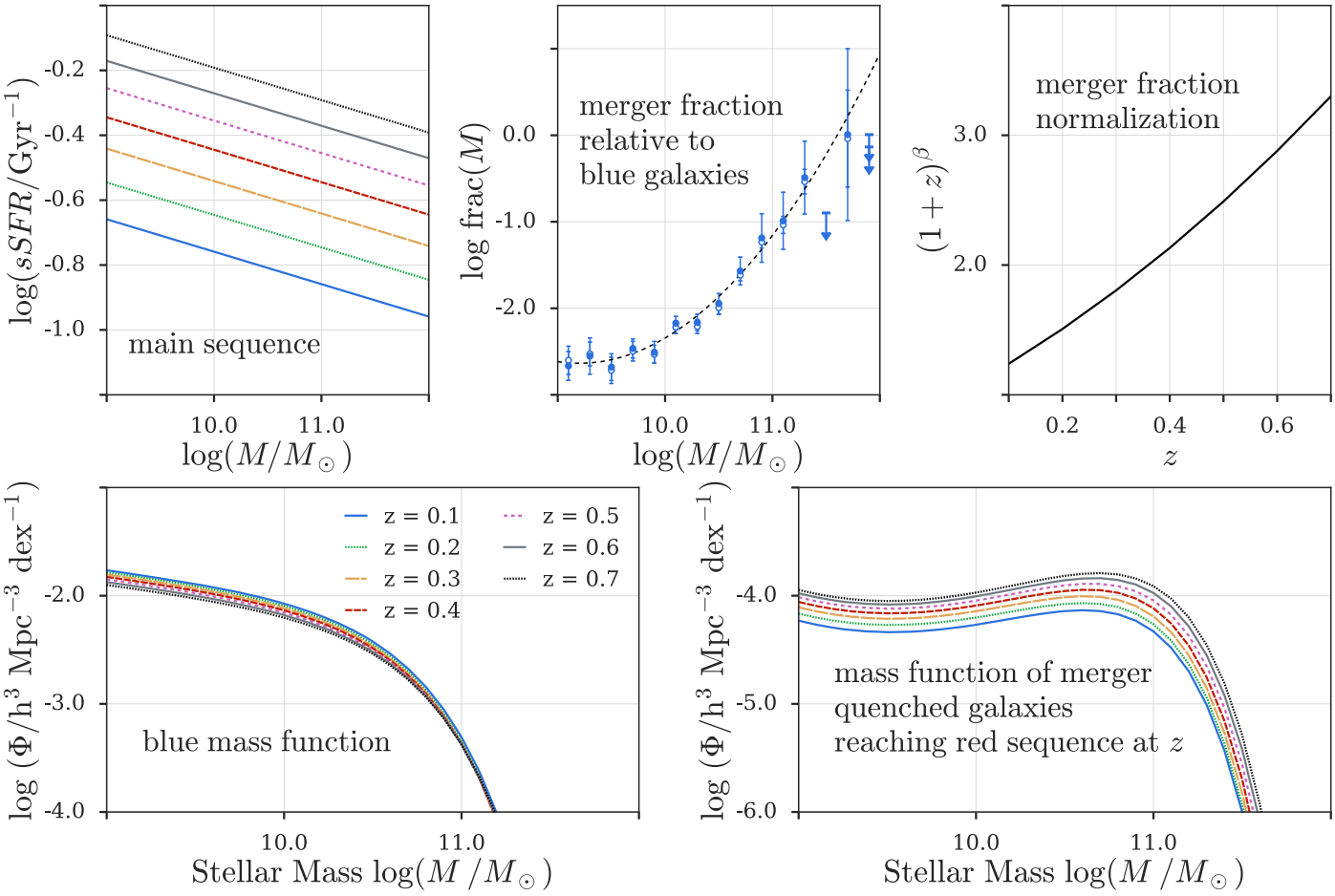

Figure 16. Input for the simple model to estimate the contribution of merger-quenched galaxies to the build-up of the red sequence within $0 < z < 0.5$ (see Section 5.6). We base our model on the redshift evolution of the blue stellar mass function (bottom left-hand panel; Caplar et al. 2015). To estimate the number density of newly quenched galaxies between z_1 and z_2 ($z_1 > z_2$), we evolve $M^*(z_1)$ along the main sequence (top right-hand panel; Lilly et al. 2013) and subtract the true, observed blue mass function at z_2 from the predicted one. We assume that it takes merger-quenched galaxies $\sim$1 Gyr to transition from the major-merger to the red early-type stage. To determine the evolution of these red merger-quenched galaxies, we parametrize the major-merger mass function as the product of the blue mass function and the merger fraction at $z \sim 0$ (central top panel). Furthermore, we ensure that the number of major mergers increases with increasing redshift by introducing a factor of $(1 + z)^{\beta}$ ($\beta = 2.25$, top right-hand panel; Bridge et al. 2010). The redshift evolution of the merger-quenched galaxies' mass function is shown in the bottom right-hand panel. Note that for the red major merger mass function at z we use $\Phi_{\rm blue}(z_{\rm mm})$ and $(1 + z_{\rm mm})$, where $z_{\rm mm} - z \triangleq 1$ Gyr. We thus show $\Phi_{\rm blue}$, the main sequence, and $(1 + z)^{\beta}$ for values beyond $z = 0.5$.

function estimates. For the stellar mass function in the left-hand panel, we used the D10 stellar mass values of the primaries as input. In the central panel, we show the merger-mass function based on the D10 mass estimates for the less massive of the two merging galaxies, the secondary. For the stellar mass function in the right-hand panel, we used the sum of the primary and the secondary as input. As spectra are only available for a subset of galaxies in the D10 sample, we use photometric redshifts if spectroscopic redshifts are unavailable. For the stellar mass function shown in the right-hand panel, we use the redshift and the apparent magnitude of the primary to determine if the merging system lies within our redshift range and to correct for mass-completeness effects (Weigel et al. 2016). In Figure 14, we show the major-merger mass function that was estimated with the approach discussed above in gray for comparison. This is the mass function that we use for our analysis.

Figure 14 shows that the merger mass functions that are solely based on the masses of the primaries and secondaries do not deviate significantly from the stellar mass function that we use for our analysis, which is generated using a mix of primary and secondary masses.

As expected, using the sum of the merging galaxies for the stellar mass function construction leads to a deviation at the steep high-mass end. To test if this shift in M^* significantly affects our analysis, we determine the ratio between the major-merger mass function and the post-merger mass function (see Section 5.1). From left to right, Figure 15 shows the major-merger mass function based on primary masses, secondary masses, and the sum of primary and secondary masses relative to the post-merger mass function. Shown in gray is the ratio between the major-merger mass function, which we use for our analysis, and the post-merger mass function. The horizontal dashed lines illustrate the best-fitting relation if we assume a constant ratio between the modified merger mass functions and the post-merger mass function. The corresponding $\chi^2_{\rm reduced}$ are shown within in the panels.

Figure 15 shows that even though using the sum of masses for the major merger mass function construction leads to a shift

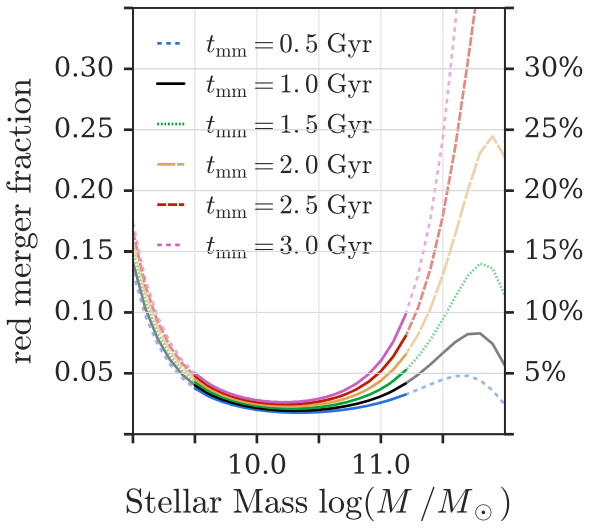

Figure 17. Contribution of major-merger-quenched galaxies to the build-up of the red sequence within the last 5 Gyr. In analogy to Figure 13, we show the fraction of red galaxies that have been quenched through major mergers as a function of stellar mass. For our model in Section 5.6, we assume that it takes galaxies of the order of $t_{\rm mm} \sim 1$ Gyr to transition from the major-merger to the red early-type stage. Here we show that our result is not significantly affected by the chosen $t_{\rm mm}$ value. Note that the low- and the high-mass end of the major-merger mass function is affected by significant uncertainties. We thus only consider stellar masses within $9.5 < \log(M/M_\odot) < 11.25$ for our model.

in M^*, the ratio between the major-merger and the post-merger mass functions still shows no significant mass dependence. Using the sum of masses for the merger mass function would thus result in a steeper mass dependence of the merger fraction (see Figure 3), but it would not significantly impact our analysis regarding major-merger quenching.

A.2. Merger Contribution to the Build-up of the Red Sequence

In Section 5.6, we determine the contribution of major-merger-quenched galaxies to the build-up of the red sequence within the last 5 Gyr. To do so, we model the redshift evolution of the major-merger mass function and estimate the number of newly quenched galaxies within a given redshift interval. In addition to Figure 13, we show the evolution of the main sequence, the merger fraction as a function of stellar mass, the redshift evolution of the normalization of the merger fraction, and the evolution of the blue mass function in Figure 16. Furthermore, we show the evolution of the mass function of galaxies that have been quenched through major mergers and reach the red sequence at a certain redshift.

For our simple model, we assume that it takes galaxies of the order of $t_{\rm mm} \sim 1$ Gyr to evolve from the major-merger to the red early-type stage. In Figure 17, we show that our estimate of the contribution of major-merger-quenched galaxies to the red sequence since $z \sim 0.5$ is not significantly affected by the chosen $t_{\rm mm}$ value.

ORCID iDs

Anna K. Weigel https://orcid.org/0000-0002-5489-4316
Kevin Schawinski https://orcid.org/0000-0001-5464-0888
Neven Caplar https://orcid.org/0000-0003-3287-5250
Alfredo Carpineti https://orcid.org/0000-0002-0334-2853
Ross E. Hart https://orcid.org/0000-0002-4893-1264
William C. Keel https://orcid.org/0000-0002-6131-9539
Sandor J. Kruk https://orcid.org/0000-0001-8010-8879
Chris J. Lintott https://orcid.org/0000-0001-5578-359X
Brooke D. Simmons https://orcid.org/0000-0001-5882-3323

References

Abazajian, K. N., Adelman-McCarthy, J. K., Agüeros, M. A., et al. 2009, ApJS, 182, 543
Adelman-McCarthy, J. K., Agüeros, M. A., Allam, S. S., et al. 2007, ApJS, 172, 634
Aird, J., Coil, A. L., Moustakas, J., et al. 2012, ApJ, 746, 90
Alexander, D. M., & Hickox, R. C. 2012, NewAR, 56, 93
Astropy Collaboration, Robitaille, T. P., Tollerud, E. J., et al. 2013, A&A, 558, A33
Baldry, I. K., Driver, S. P., Loveday, J., et al. 2012, MNRAS, 421, 621
Baldry, I. K., Glazebrook, K., Brinkmann, J., et al. 2004, ApJ, 600, 681
Balogh, M. L., Navarro, J. F., & Morris, S. L. 2000, ApJ, 540, 113
Bamford, S. P., Nichol, R. C., Baldry, I. K., et al. 2009, MNRAS, 393, 1324
Barnes, J. E. 2002, MNRAS, 333, 481
Barnes, J. E., & Hernquist, L. 1996, ApJ, 471, 115
Behroozi, P. S., Wechsler, R. H., & Conroy, C. 2013, ApJ, 770, 57
Bekki, K., Shioya, Y., & Couch, W. J. 2001, ApJL, 547, L17
Bell, E. F., McIntosh, D. H., Katz, N., & Weinberg, M. D. 2003, ApJS, 149, 289
Bell, E. F., Wolf, C., Meisenheimer, K., et al. 2004, ApJ, 608, 752
Bennert, N., Canalizo, G., Jungwiert, B., et al. 2008, ApJ, 677, 846
Bertone, S., & Conselice, C. J. 2009, MNRAS, 396, 2345
Birnboim, Y., Dekel, A., & Neistein, E. 2007, MNRAS, 380, 339
Bland-Hawthorn, J. 2015, in IAU Symp. 309, Galaxies in 3D Across the Universe, ed. B. L. Ziegler et al. (Cambridge: Cambridge Univ. Press), 21
Blanton, M. R., & Roweis, S. 2007, AJ, 133, 734
Blanton, M. R., Schlegel, D. J., Strauss, M. A., et al. 2005, AJ, 129, 2562
Bois, M., Bournaud, F., Emsellem, E., et al. 2010, MNRAS, 406, 2405
Bois, M., Emsellem, E., Bournaud, F., et al. 2011, MNRAS, 416, 1654
Bongiorno, A., Schulze, A., Merloni, A., et al. 2016, A&A, 588, A78
Bournaud, F. 2011, in EAS Publications Ser. 51, ed. C. Charbonnel & T. Montmerle (Les Ulis: EDP Sciences), 107
Bridge, C. R., Carlberg, R. G., & Sullivan, M. 2010, ApJ, 709, 1067
Brinchmann, J., Charlot, S., White, S. D. M., et al. 2004, MNRAS, 351, 1151
Bruzual, G., & Charlot, S. 2003, MNRAS, 344, 1000
Bryant, J. J., Owers, M. S., Robotham, A. S. G., et al. 2015, MNRAS, 447, 2857
Bundy, K., Bershady, M. A., Law, D. R., et al. 2015, ApJ, 798, 7
Bundy, K., Fukugita, M., Ellis, R. S., et al. 2009, ApJ, 697, 1369
Calzetti, D., Armus, L., Bohlin, R. C., et al. 2000, ApJ, 533, 682
Caplar, N., Lilly, S. J., & Trakhtenbrot, B. 2015, ApJ, 811, 148
Cappellari, M. 2016, ARA&A, 54, 597
Cappellari, M., Emsellem, E., Krajnović, D., et al. 2011, MNRAS, 413, 813
Carpineti, A., Kaviraj, S., Darg, D., et al. 2012, MNRAS, 420, 2139
Carpineti, A., Kaviraj, S., Hyde, A. K., et al. 2015, A&A, 577, A119
Casteels, K. R. V., Conselice, C. J., Bamford, S. P., et al. 2014, MNRAS, 445, 1157
Catinella, B., Schiminovich, D., Kauffmann, G., et al. 2010, MNRAS, 403, 683
Cattaneo, A., Faber, S. M., Binney, J., et al. 2009, Natur, 460, 213
Chandrasekhar, S. 1943, ApJ, 97, 255
Cheung, E., Athanassoula, E., Masters, K. L., et al. 2013, ApJ, 779, 162
Conselice, C. J. 2003, ApJS, 147, 1
Croom, S. M., Lawrence, J. S., Bland-Hawthorn, J., et al. 2012, MNRAS, 421, 872
Croton, D. J., Springel, V., White, S. D. M., et al. 2006, MNRAS, 365, 11
Daddi, E., Bournaud, F., Walter, F., et al. 2010, ApJ, 713, 686
Daddi, E., Dickinson, M., Morrison, G., et al. 2007, ApJ, 670, 156
Darg, D. W., Kaviraj, S., Lintott, C. J., et al. 2010a, MNRAS, 401, 1043
Darg, D. W., Kaviraj, S., Lintott, C. J., et al. 2010b, MNRAS, 401, 1552
Davies, R. L., Efstathiou, G., Fall, S. M., Illingworth, G., & Schechter, P. L. 1983, ApJ, 266, 41
De Lucia, G., Fontanot, F., Wilman, D., & Monaco, P. 2011, MNRAS, 414, 1439
de Zeeuw, P. T., Bureau, M., Emsellem, E., et al. 2002, MNRAS, 329, 513
Di Matteo, P., Bournaud, F., Martig, M., et al. 2008, A&A, 492, 31
Di Matteo, T., Springel, V., & Hernquist, L. 2005, Natur, 433, 604
Domingue, D. L., Xu, C. K., Jarrett, T. H., & Cheng, Y. 2009, arXiv:0901.4545
Efstathiou, G., Ellis, R. S., & Peterson, B. A. 1988, MNRAS, 232, 431
Elbaz, D., Daddi, E., Le Borgne, D., et al. 2007, A&A, 468, 33

Ellison, S. L., Fertig, D., Rosenberg, J. L., et al. 2015, MNRAS, 448, 221
Ellison, S. L., Mendel, J. T., Patton, D. R., et al. 2013, MNRAS, 453, 3627
Ellison, S. L., Patton, D. R., Mendel, J. T., & Scudder, J. M. 2011, MNRAS, 418, 2043
Ellison, S. L., Patton, D. R., Simard, L., & McConnachie, A. W. 2008, AJ, 135, 1877
Faber, S. M., Willmer, C. N. A., Wolf, C., et al. 2007, ApJ, 665, 265
Fabian, A. C. 2012, ARA&A, 50, 455
Faisst, A., Carollo, C. M., Capak, P., et al. 2017, ApJ, 839, 71
Fang, J. J., Faber, S. M., Salim, S., Graves, G. J., & Rich, R. M. 2012, ApJ, 761, 23
Forbes, D. A., Romanowsky, A. J., Pastorello, N., et al. 2016, MNRAS, 457, 1242
French, K. D., Yang, Y., Zabludoff, A., et al. 2015, ApJ, 801, 1
Gawiser, E., van Dokkum, P. G., Herrera, D., et al. 2006, ApJS, 162, 1
Genzel, R., Lutz, D., Sturm, E., et al. 1998, ApJ, 498, 579
Genzel, R., Tacconi, L. J., Rigopoulou, D., Lutz, D., & Tecza, M. 2001, ApJ, 563, 527
Georgakakis, A., Nandra, K., Yan, R., et al. 2008, MNRAS, 385, 2049
George, K. 2017, A&A, 598, A45
Goto, T. 2005, MNRAS, 357, 937
Governato, F., Brook, C. B., Brooks, A. M., et al. 2009, MNRAS, 398, 312
Gunn, J. E., & Gott, J. R., III 1972, ApJ, 176, 1
Hart, R. E., Bamford, S. P., Willett, K. W., et al. 2016, MNRAS, 461, 3663
Hau, G. K. T., Bower, R. G., Kilborn, V., et al. 2008, MNRAS, 385, 1965
Hernquist, L. 1989, Natur, 340, 687
Hernquist, L., & Barnes, J. E. 1991, Natur, 354, 210
Hickox, R. C., Jones, C., Forman, W. R., et al. 2009, ApJ, 696, 891
Hong, J., Im, M., Kim, M., & Ho, L. C. 2015, ApJ, 804, 34
Hopkins, P. F., Bundy, K., Croton, D., et al. 2010a, ApJ, 715, 202
Hopkins, P. F., Cox, T. J., Kereš, D., & Hernquist, L. 2008a, ApJS, 175, 390
Hopkins, P. F., Cox, T. J., Younger, J. D., & Hernquist, L. 2009, ApJ, 691, 1168
Hopkins, P. F., Croton, D., Bundy, K., et al. 2010b, ApJ, 724, 915
Hopkins, P. F., Hernquist, L., Cox, T. J., et al. 2006, ApJS, 163, 1
Hopkins, P. F., Hernquist, L., Cox, T. J., & Kereš, D. 2008b, ApJS, 175, 356
Hunter, J. D. 2007, CSE, 9, 90
Ilbert, O., McCracken, H. J., Le Fèvre, O., et al. 2013, A&A, 556, A55
Illingworth, G. 1977, ApJL, 218, L43
Jannuzi, B. T., & Dey, A. 1999, in ASP Conf. Ser. 191, Photometric Redshifts and the Detection of High Redshift Galaxies, ed. R. Weymann (San Francisco, CA: ASP), 111
Jarrett, T. H., Chester, T., Cutri, R., et al. 2000, AJ, 119, 2498
Jiang, C. Y., Jing, Y. P., Faltenbacher, A., Lin, W. P., & Li, C. 2008, ApJ, 675, 1095
Jiang, C. Y., Jing, Y. P., & Lin, W. P. 2010, A&A, 510, A60
Jogee, S. 2006, in Physics of Active Galactic Nuclei at all Scales, ed. D. Alloin (Berlin: Springer), 143
Kannappan, S. J., Guie, J. M., & Baker, A. J. 2009, AJ, 138, 579
Kauffmann, G., Heckman, T. M., Budavári, T., et al. 2007, ApJS, 173, 357
Kauffmann, G., Heckman, T. M., White, S. D. M., et al. 2003, MNRAS, 341, 33
Kaviraj, S. 2014, MNRAS, 440, 2944
Kaviraj, S., Kirkby, L. A., Silk, J., & Sarzi, M. 2007, MNRAS, 382, 960
Kaviraj, S., Laigle, C., Kimm, T., et al. 2017, MNRAS, 467, 4739
Kaviraj, S., Schawinski, K., Silk, J., & Shabala, S. S. 2011, MNRAS, 415, 3798
Kaviraj, S., Shabala, S. S., Deller, A. T., & Middelberg, E. 2015, MNRAS, 452, 774
Keenan, R. C., Foucaud, S., De Propris, R., et al. 2014, ApJ, 795, 157
Khalatyan, A., Cattaneo, A., Schramm, M., et al. 2008, MNRAS, 387, 13
Khochfar, S., Emsellem, E., Serra, P., et al. 2011, MNRAS, 417, 845
Knobel, C., Lilly, S. J., Woo, J., & Kovač, K. 2015, ApJ, 800, 24
Komatsu, E., Smith, K. M., Dunkley, J., et al. 2011, ApJS, 192, 18
Kormendy, J., & Kennicutt, R. C., Jr. 2004, ARA&A, 42, 603
Koss, M., Mushotzky, R., Veilleux, S., et al. 2011, ApJ, 739, 57
Koss, M., Mushotzky, R., Veilleux, S., & Winter, L. 2010, ApJL, 716, L125
Kurczynski, P., Gawiser, E., Acquaviva, V., et al. 2016, ApJL, 820, L1
Land, K., Slosar, A., Lintott, C., et al. 2008, MNRAS, 388, 1686
Larson, R. B., Tinsley, B. M., & Caldwell, C. N. 1980, ApJ, 237, 692
Lee, N., Sanders, D. B., Casey, C. M., et al. 2015, ApJ, 801, 80
Li, C., & White, S. D. M. 2009, MNRAS, 398, 2177
Lilly, S. J., Carollo, C. M., Pipino, A., Renzini, A., & Peng, Y. 2013, ApJ, 772, 119
Lintott, C., Schawinski, K., Bamford, S., et al. 2011, MNRAS, 410, 166
Lintott, C. J., Schawinski, K., Slosar, A., et al. 2008, MNRAS, 389, 1179
Lofthouse, E. K., Kaviraj, S., Conselice, C. J., et al. 2017, MNRAS, 465, 2895
Lotz, J. M., Jonsson, P., Cox, T. J., et al. 2011, ApJ, 742, 103
Lotz, J. M., Primack, J., & Madau, P. 2004, AJ, 128, 163
Maraston, C. 1998, MNRAS, 300, 872
Maraston, C. 2005, MNRAS, 362, 799
Martin, D. C., Wyder, T. K., Schiminovich, D., et al. 2007, ApJS, 173, 342
Masters, K. L., Mosleh, M., Romer, A. K., et al. 2010, MNRAS, 405, 783
Masters, K. L., Nichol, R. C., Hoyle, B., et al. 2011, MNRAS, 411, 2026
Mihos, J. C., & Hernquist, L. 1996, ApJ, 464, 641
Moffett, A. J., Kannappan, S. J., Baker, A. J., & Laine, S. 2012, ApJ, 745, 34
Muzzin, A., Marchesini, D., Stefanon, M., et al. 2013, ApJ, 777, 18
Naab, T., Jesseit, R., & Burkert, A. 2006, MNRAS, 372, 839
Naab, T., Oser, L., Emsellem, E., et al. 2014, MNRAS, 444, 3357
Noeske, K. G., Weiner, B. J., Faber, S. M., et al. 2007, ApJL, 660, L43
Oh, K., Sarzi, M., Schawinski, K., & Yi, S. K. 2011, ApJS, 195, 13
Oh, S., Yi, S. K., Cortese, L., et al. 2016, arXiv:1609.03595
Ostriker, J. P. 1980, ComAp, 8, 177
Padmanabhan, N., Schlegel, D. J., Finkbeiner, D. P., et al. 2008, ApJ, 674, 1217
Patton, D. R., Carlberg, R. G., Marzke, R. O., et al. 2000, ApJ, 536, 153
Patton, D. R., Pritchet, C. J., Yee, H. K. C., Ellingson, E., & Carlberg, R. G. 1997, ApJ, 475, 29
Peng, Y., Maiolino, R., & Cochrane, R. 2015, Natur, 521, 192
Peng, Y.-J., Lilly, S. J., Kovač, K., et al. 2010, ApJ, 721, 193
Peng, Y.-j., Lilly, S. J., Renzini, A., & Carollo, M. 2012, ApJ, 757, 4
Pozzetti, L., Bolzonella, M., Zucca, E., et al. 2010, A&A, 523, A13
Robertson, B., Bullock, J. S., Cox, T. J., et al. 2006, ApJ, 645, 986
Robertson, B. E., & Bullock, J. S. 2008, ApJL, 685, L27
Robotham, A. S. G., Driver, S. P., Davies, L. J. M., et al. 2014, MNRAS, 444, 3986
Rodriguez-Gomez, V., Sales, L. V., Genel, S., et al. 2016, arXiv:1609.09498
Salim, S., Fang, J. J., Rich, R. M., Faber, S. M., & Thilker, D. A. 2012, ApJ, 755, 105
Salim, S., Rich, R. M., Charlot, S., et al. 2007, ApJS, 173, 267
Salpeter, E. E. 1955, ApJ, 121, 161
Sánchez, S. F., Kennicutt, R. C., Gil de Paz, A., et al. 2012, A&A, 538, A8
Sandage, A., Tammann, G. A., & Yahil, A. 1979, ApJ, 232, 352
Sanders, D. B., & Mirabel, I. F. 1996, ARA&A, 34, 749
Sanders, D. B., Soifer, B. T., Elias, J. H., et al. 1988, ApJ, 325, 74
Schawinski, K., Dowlin, N., Thomas, D., Urry, C. M., & Edmondson, E. 2010, ApJL, 714, L108
Schawinski, K., Khochfar, S., Kaviraj, S., et al. 2006, Natur, 442, 888
Schawinski, K., Lintott, C., Thomas, D., et al. 2009, MNRAS, 396, 818
Schawinski, K., Thomas, D., Sarzi, M., et al. 2007, MNRAS, 382, 1415
Schawinski, K., Urry, C. M., Simmons, B. D., et al. 2014, MNRAS, 440, 889
Schechter, P. 1976, ApJ, 203, 297
Schmidt, M. 1968, ApJ, 151, 393
Silk, J., & Rees, M. J. 1998, A&A, 331, L1
Simmons, B. D., Lintott, C., Schawinski, K., et al. 2013, MNRAS, 429 2199
Smethurst, R. J., Lintott, C. J., Simmons, B. D., et al. 2015, MNRAS, 450 435
Smethurst, R. J., Lintott, C. J., Simmons, B. D., et al. 2016, MNRAS, 463, 2986
Somerville, R. S., Hopkins, P. F., Cox, T. J., Robertson, B. E., & Hernquist, L. 2008, MNRAS, 391, 481
Sparre, M., & Springel, V. 2016, arXiv:1610.03850
Speagle, J. S., Steinhardt, C. L., Capak, P. L., & Silverman, J. D. 2014, ApJS, 214, 15
Springel, V., Di Matteo, T., & Hernquist, L. 2005a, ApJL, 620, L79
Springel, V., Di Matteo, T., & Hernquist, L. 2005b, MNRAS, 361, 776
Springel, V., & Hernquist, L. 2005, ApJL, 622, L9
Tacconi, L. J., Genzel, R., Neri, R., et al. 2010, Natur, 463, 781
Taylor, E. N., Hopkins, A. M., Baldry, I. K., et al. 2015, MNRAS, 446 2144
Tomczak, A. R., Quadri, R. F., Tran, K.-V. H., et al. 2016, ApJ, 817, 118
Toomre, A., & Toomre, J. 1972, ApJ, 178, 623
Treister, E., Schawinski, K., Urry, C. M., & Simmons, B. D. 2012, ApJL, 758, L39
Tremonti, C. A., Moustakas, J., & Diamond-Stanic, A. M. 2007, ApJL, 663, L77
Ueda, J., Iono, D., Yun, M. S., et al. 2014, ApJS, 214, 1
Urrutia, T., Lacy, M., & Becker, R. H. 2008, ApJ, 674, 80
van Dokkum, P. G. 2005, AJ, 130, 2647
Weigel, A. K., Schawinski, K., & Bruderer, C. 2016, MNRAS, 459 2150

Weigel, A. K., Schawinski, K., Caplar, N., et al. 2017, e-print (arXiv:1707.05323)
Willett, K. W., Lintott, C. J., Bamford, S. P., et al. 2013, MNRAS, 435, 2835
Willett, K. W., Schawinski, K., Simmons, B. D., et al. 2015, MNRAS, 449, 820
Willmer, C. N. A. 1997, AJ, 114, 898
Wong, O. I., Schawinski, K., Józsa, G. I. G., et al. 2015, MNRAS, 447 3311
Wong, O. I., Schawinski, K., Kaviraj, S., et al. 2012, MNRAS, 420, 1684
Woo, J., Dekel, A., Faber, S. M., & Koo, D. C. 2015, MNRAS, 448, 237
Xu, C. K., Sun, Y. C., & He, X. T. 2004, ApJL, 603, L73
Xu, C. K., Zhao, Y., Scoville, N., et al. 2012, ApJ, 747, 85
Yamauchi, C., Yagi, M., & Goto, T. 2008, MNRAS, 390, 383
Yan, R., Newman, J. A., Faber, S. M., et al. 2006, ApJ, 648, 281
Yang, X., Mo, H. J., van den Bosch, F. C., et al. 2007, ApJ, 671, 153
York, D. G., Adelman, J., Anderson, J. E., Jr., et al. 2000, AJ, 120 1579
Yuan, T.-T., Kewley, L. J., & Sanders, D. B. 2010, ApJ, 709, 884